UNIVERSITY OF CALIFORNIA
RIVERSIDE

Continuous High-Throughput Cell Sorting Using Density

A Dissertation submitted in partial satisfaction
of the requirements for the degree of

Doctor of Philosophy

in

Bioengineering

by

Nazila Norouzi

December 2016

Dissertation Committee:

Dr. William H. Grover, Chairperson
Dr. Dimitri Morikis
Dr. Hyle Park

The Dissertation of Nazila Norouzi is approved:

Committee Chairperson

University of California, Riverside

Acknowledgments

I am grateful to my advisor, without whose help, I would not have been here.

To my husband and my parents for all the support.

ABSTRACT OF THE DISSERTATION

Continuous High-Throughput Cell Sorting Using Density

by

Nazila Norouzi

Doctor of Philosophy, Graduate Program in Bioengineering
University of California, Riverside, December 2016
Dr. William H. Grover, Chairperson

Sorting cells by their type is an important capability in biological research and medical diagnostics. However, most cell sorting techniques rely on labels, which may have limited availability and specificity. Sorting different cell types by their different physical properties is an attractive alternative to labels because all cells intrinsically have these physical properties. But for some physical properties like cell size, the relatively large cell-to-cell variation within a cell type can make it difficult to identify and sort cells based on their size. In this work we sort different cells types by their density, a physical property with much lower cell-to-cell variation within a cell type (and therefore greater potential to discriminate different cell types) than other physical properties. We accomplish this using a 3D-printed microfluidic chip containing a flowing micron-scale density gradient. Earth's gravity makes each cell in the gradient quickly float or sink to the point where the cell's density matches the surrounding fluid's density, after which the cells are routed to different outlets and therefore sorted by their density. As a proof of concept, we use our density sorter chip to sort polymer microbeads by their material (polyethylene and

polystyrene) and blood cells by their type (white blood cells and red blood cells). The simplicity, resolution, and throughput of this technique make it suitable for isolating even rare cell types in complex biological samples, in a wide variety of different research and clinical applications. We also demonstrated a technique for controlling microfluidic chips that requires no off-chip hardware. We accomplish this by using inert compounds to adjust the densities of fluids in the chip. When fluids of different densities flow together under laminar flow, the interface between the fluids quickly reorients to be orthogonal to Earth's gravitational force. If the channel containing the fluids then splits into two channels, the amount of each fluid flowing into each channel is precisely determined by the angle of the channels relative to gravity. This approach allows for sophisticated control of on-chip fluids with no off-chip control hardware, significantly reducing the cost of microfluidic instruments in point-of-care or resource-limited settings.

Contents

List of Figures

List of Tables

Chapter 1

Introduction

Cancer has become the second most likely cause of death worldwide. The most deadly aspect of cancer is its ability to spread or metastasize. In metastasis, cancer cells break away from a primary tumor, travel through the body in the circulatory system, and potentially establish new tumors elsewhere in the body. Metastasis is a very complicated process that still has yet to be completely understood. [1]

In early tumor expansion, growing tumor cells rapidly outstrip the supply of nutrients and activate angiogenesis. Angiogenesis is regulated by angiogenic, growth, and survival factors that are secreted by the malignant cells as well as other cells within the tumor microenvironment. Cell adhesion is reduced which causes tumor cells detachment and resistance to apoptosis and causes invading tumor cells to undergo the "epithelial to mesenchymal transition" (EMT) phenotype switch, which causes them to lose epithelial antigens and acquire mesenchymal antigens and motile propensities. After entering blood vessels (intravasation), circulating tumor cells (CTCs) circulate as isolated CTCs

extravasate to distant organs or give rise to metastases when they migrate and arrest in capillaries and proliferate, rupturing the capillary walls. After extravasation, CTCs remain as dormant solitary cells (disseminated tumor cells, DTC), or undergo limited proliferation (micrometastases) which give rise to metastases, via phenotype reversion mesenchymal to epithelial transition (MET) and angiogenesis (1.1A-E). [2]

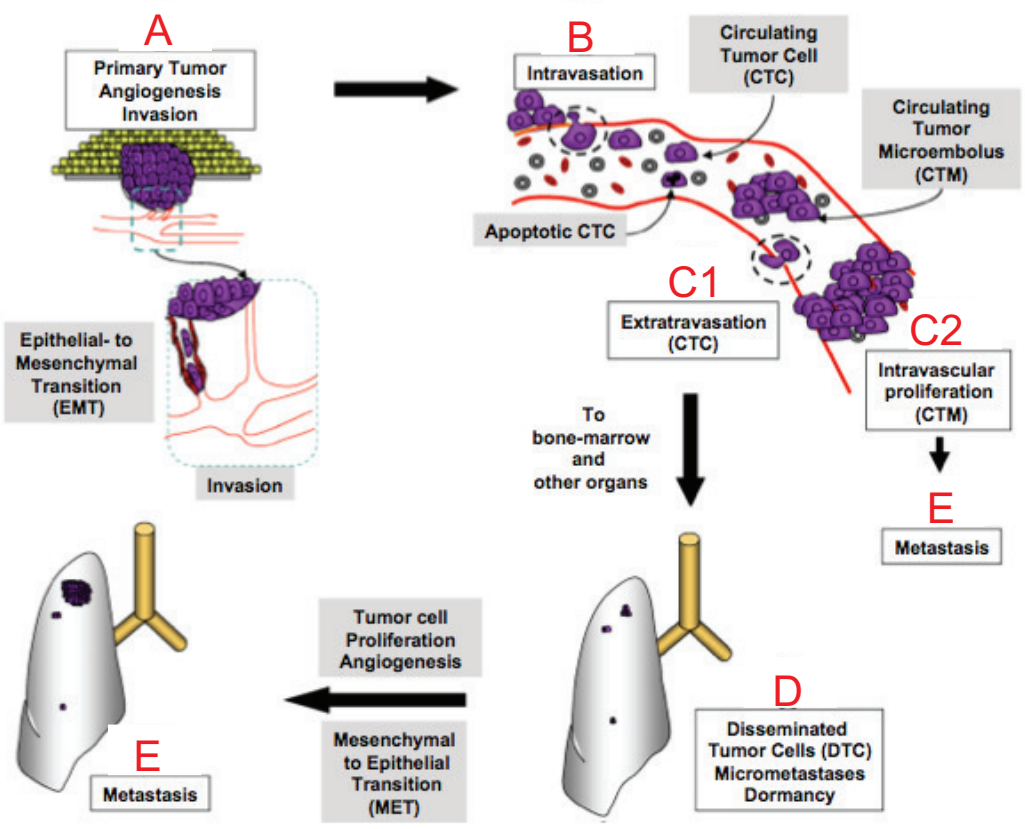

Figure 1.1: Main steps leading to development of metastases. [2]

Since the dissemination of cancer cells mainly occurs through the bloodstream, CTCs that have been shed into the vasculature are of obvious interest with many studies indicating their potential value in cancer prognosis, therapy monitoring, anticancer drugs,

and metastasis research [3, 4]. It has been estimated that around 10^6 tumor cells per gram of tumor tissue can be introduced daily into the bloodstream. [5] The technical challenge in this field consists of finding rare tumor cells (just a few CTCs mixed with the approximately 10 million leukocytes and 5 billion erythrocytes in one milliliter of blood) and being able to distinguish them from epithelial non-tumor cells and leukocytes.

The challenge of CTC detection is largely due to the requirement of high **sensitivity** combined with high **specificity**. Since invasion can start very early during tumor development, identification and counting of CTCs when they are very rare (a few CTCs per 10 mL of blood) could alert the oncologist about a developing tumor invasion process. Specificity is also an absolute requirement in this field. In fact, a wrong identification of non-tumor cells (such as epithelial non-tumor cells) as "tumor cells" could generate poor clinical and therapeutical choices having a negative impact on the quality and/or expectancy of life in patients with cancer. A variety of analytical tools have been developed in recent years to improve the ability of detecting and isolating these rare cells. The main methods of CTC detection and separation are described below.

1.1 Commercial CTC Separation Micro-systems

Semi-automated micro-scale commercial systems such as Ficoll, OncoQuick and CellSearch have been developed for CTC isolation in recent years. These systems could be beneficial for cancer patients throughout the therapy since the testings results can be used to monitor a patient's status by indicating whether their prognosis on a given therapy is favorable or unfavorable at a given time.

Ficoll-hypaque. Ficoll-hypaque is a CTC enrichment technique based on cell density gradient centrifugation. The basis for this cell separation assay is the differential migration of cells during centrifugation according to their densities, which results in the separation of different cell types into distinct layers. After centrifugation, the cells stratify into layers (from most dense on the bottom to least dense on the top) of erythrocytes, neutrophils, density gradient, mononuclear cells (lymphocytes, monocytes, epithelial cells, tumor cells), and finally plasma on the top. However, tumor cells can migrate into the plasma fraction, and whole blood rapidly starts to mix with the density gradient if it is not immediately separated. Both of these phenomena can prevent optimal cell separation in ficoll-hypaque. [6]

OncoQuick. The commercially-available OncoQuick assay (Greiner, Frickenhausen, Germany) was developed to enhance the efficiency of Ficoll enrichment technique. Unlike the Ficoll technique, OncoQuick has the advantage of a porous barrier that separates the separation medium from the sample before centrifugation Figure (1.2A). This technique has been designed to isolate mononuclear cells with low density cells and particles (low density leukocytes, epithelial cells, tumor cells, platelets) from neutrophils and lymphocytes and capture CTCs. The tubes permit the layering of whole blood (15–35 mL) on the porous barrier, thus avoiding mixing the blood with the density gradient before centrifugation. [6]

The OncoQuick technique allows for greater enrichment of tumor cells from leukocytes, which simplifies further analyses such as cell staining, immunolabelling, and molecular studies. The limiting problem of the OncoQuick system is that rare CTCs can be lost during the isolation step as they can migrate into the plasma fraction or become trapped among

erythrocytes and neutrophils [7, 8], so the system has very low and variable sensitivity, purity, and enrichments depending on tumor cell characteristics, centrifuge time, temperature, and other factors. [9, 10]

CellSearch. The CellSearch assay (Figure. 2B) uses ferrofluid nanoparticles coated with epithelial cell-specific antibody (anti-EpCAM) to immunomagnetically enrich epithelial cells. A 7.5 mL sample of blood is placed in a special tube and centrifuged to separate solid blood components from plasma. The CTCs are then magnetically separated from the bulk of other cells and then permeabilized with the fluorescent nuclear dye DAPI (to identify CD45, a marker specific to leukocytes which identifies any leukocytes) and fluorescent antibodies to intracellular cytokeratins (CK) specific to epithelial cells. Sample analysis is performed by the CellSpotter, a four color semi-automated fluorescence microscope which identifies epithelial cells from being positive for the CK markers and negative for the CD45 marker.

The advantage of the CellSearch assay is that it is more sensitive than the Oncoquick method, semi-automated, has reduced trapping of leucocytes with epithelial cells, and allows for cell counting. [11, 6] However, cell isolation and detection are performed with antibodies specific to epithelial cells (EpCAM, Cytokeratins 8, 18, and 19) and since epithelial non-tumor cells can be spread in the peripheral blood, it is difficult to determine, in a given patient having a certain number of circulating epithelial cells (CEpC), what is the actual number of tumor cells. This is particularly relevant when CTC counting is performed to assess the response of a tumor to therapy or the risk of developing tumor

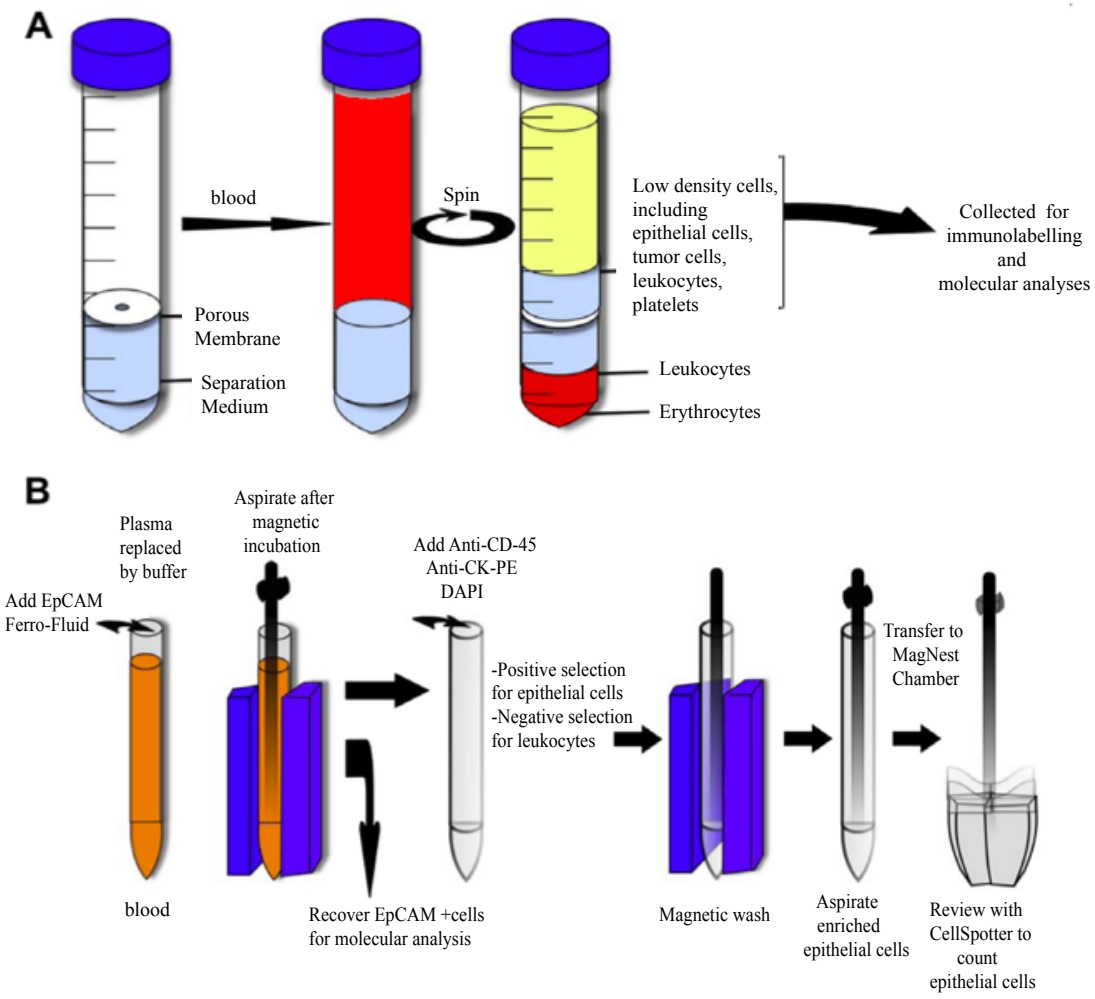

Figure 1.2: Examples of commercially available methods to isolate circulating tumor cells. **(A)** Oncoquick. Tumor cells, epithelial cells, platelets and low density leukocytes are enriched from leukocytes and erythrocytes based on their particular density. They can then be collected for cytopathological analyses, immunolabelling and molecular studies. **(B)** CellSearch. Blood cells expressing epithelial antigens (EpCAM) are captured by EpCAM-bound ferrofluid. They can be recovered for molecular analysis or permeabilized and submitted to a negative selection with CD45 antibody (to capture leukocytes) and to a positive selection with antibodies specific to Cytokeratins 8, 18, 19 bound to ferrofluid. After washing, cells expressing epithelial antigens are transferred to the MagNest chamber and counted with CellSpotter. [9,11]

recurrence, and in cancer screening protocols. Also, stains and labels make the CellSearch approach unsuitable for use as a therapeutic: blood that has been "cleaned" of CTCs using the CellSearch system cannot be infused back into a patient. Finally, circulating tumor micro emboli (CTM), which have a high metastasis potential, cannot be reliably detected by the CellSearch technique, as the multiple cell labeling steps and treatments with magnetic particles tend to dissociate tumor cell aggregates.

Filtration. Isolation by Size of Epithelial Tumor cells (ISET) is a blood filtration technique which is based on the fact that the majority of peripheral blood leukocytes (lymphocytes and neutrophils) are small, having a size ranging from 8 to 11 μm with a very compact nucleus. Consequently, these cells can be eliminated by filtration. Large cells remain isolated on the filter, where they can be stained with cytological stains (May-Grunwald Giemsa) or characterized by immunolabelling (TUNEL assays) in order to analyze their antigens. The simplicity of the assay avoids losing rare cells during multi-step processes and permits the precise counting of the number of CTCs/CMTs per milliliter of blood independent of the volume of blood treated. However, the use of stains and labels compromises cell viability for further studies.

1.2 Microfluidic CTC separation and detection systems

Microfluidic CTC separation and detection systems have shown promising results compared to previous methods. Microfluidic systems allow for purification of live cells with minimal damage to the cells. They allow for higher CTC recovery which enables further molecular studies on CTCs and monitoring patients' progress during treatment.

Magnetic-based Separation. In magnetic-based separation, the blood sample is combined with magnetic nanoparticles that are functionalized with an antibody to the surface of epithelial cells (anti-epithelial cell adhesion molecule, EpCAM). The cancer cells in the blood actively bind to the particles and are collected by a permanent magnet which is placed under the microfluidic channel as the blood is pumped through the microchip Figure (1.3). Compared to the commercially available CellSearch system, magnetic-based separation requires 25% fewer magnetic particles to achieve a comparable capture rate. [12]

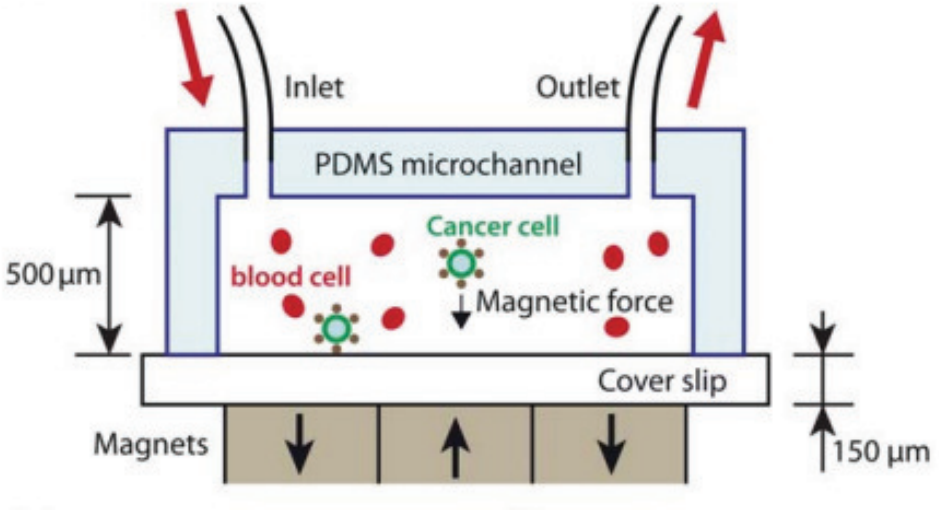

Figure 1.3: Microchip design for magnetic-based immunomagnetic detection of cancer cells. [13]

Magnetic-based separation is a continuous flow sorting technique, which means that sorting efficiency and selectivity are important factors in the technique's performance. Magnetic-bead based approaches can only isolate fixed, non-viable cells with very low purity (0.01%–0.1%) and therefore have not demonstrated clinical utility (retrieval of viable CTCs for further molecular characterization and analysis). Instead, magnetic-based techniques

have found use primarily as gross prognostic tools for classifying patients into high- and low-risk categories. [13] Furthermore, this method cannot be applied to all types of cancers, and different binding molecules require different optimal operating parameters to provide sufficient interaction time for the binding of targeted cells to occur. Not all cancers have suitable markers and known binding kinetics. For example, Siewarts *et al.* found relatively low expression levels of EpCAM on various breast cancer cell lines, even though anti-EpCAM is routinely used for enumeration of CTCs in breast cancer patients. Finally, the multiple batch processing steps involved in magnetic-based separation results in substantial loss of CTCs. [14]

Cell-affinity micro-chromatography. Cell-affinity chromatography is a method that selectively captures suspended cancer cells from a heterogeneous cell population through selective binding with substrate-immobilized high-affinity ligands, thereby isolating cancer cells from healthy cells. While the magnetic-based methods use the same interactions to bind magnetic particles to CTCs, affinity chromatography does not require CTCs to be labeled, and antibodies are attached only to the solid chromatographic surface.

A variety of different cell-affinity micro-chromatography techniques have been developed for isolating CTCs from peripheral blood. Using anti-EpCAM antibodies coated on microposts, herringbone grooves, or nano-pillars in a microfluidic chip, effective isolation of CTCs from whole blood is achieved in a single processing step (Figure 1.4). Although these micro-chromatography methods increased the capture of CTCs, the specificity of the biomarkers is the major limitation of this technique since the selection of a suitable molecule

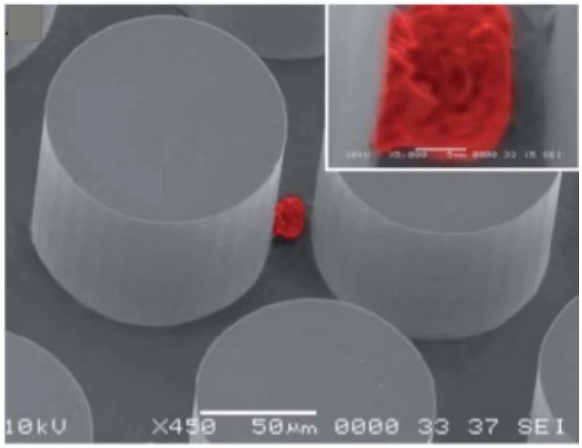

Figure 1.4: Cell-affinity micro-chromatography for cancer capture. Micro-pillars on a microfluidic CTC-chip captured a NCI-H1650 lung cancer cell (red) spiked into blood. [14]

is crucial for an effective separation. [15, 16, 17]

Dielectrophoresis. Dielectrophoresis (DEP) uses the polarization of cells in non-uniform electrical fields to exert forces on the cells. DEP forces depend on factors such as the electrical properties of the cell membrane and cytoplasm as well as the size of the cell. This technique can separate cells without the use of immunolabelling. [18]

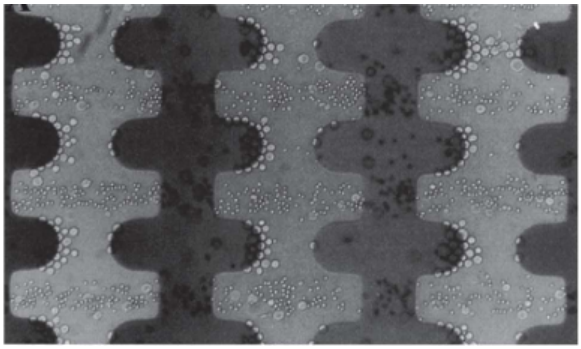

Figure 1.5: A dielectrophoretic affinity column for cancer cell separation. Large cancer cells are trapped on electrode tips while small blood cells are eluted. [18]

Using DEP, human epithelial cancer cells suspended within normal blood cells were retained on microelectrode arrays while normal blood cells were eluted. The cancer cells were subsequently released for collection by removing the DEP field. However, due to the limited dielectric differences between target cells and carrier cells, the yield and purity of DEP techniques are not high, and cell viability after DEP separation is a concern.

Dynamic lateral displacement. In addition to having different densities, leukocytes and erythrocytes are also structurally different in terms of shape and size. Leukocytes are spherical nucleated cells with typical diameters ranging from 6 μm to 10 μm. In contrast, erythrocytes or red blood cells (RBCs) have a biconcave disc-like structure with an average diameter of 7–8 μm and 2–3 μm thickness. Consequently, several microfluidic techniques have been developed that separate these cells based on their different retention and cell movement in a microfluidic chip. [15, 16, 17]

Deterministic lateral displacement (DLD) or "bump array" microfluidic chips contain arrays of micro-pillar structures as shown in Figure 1.6. Cells larger than a critical diameter (twice the width of streamlines between the pillars) follow a deterministic path and are moved by hydrodynamic lateral drag (bumped) into the sequential streamlines at each post. In contrast, smaller cells remain unperturbed and follow an average downward flow direction through the chip. DLD was successfully applied for fractionating blood components by tailoring the design to match the sizes of the blood cells. In addition to achieving 110-fold leukocyte enrichment, the device was capable of fractionating the individual white blood cell components. However, the processing rate of 1 μL/h results in an extremely low

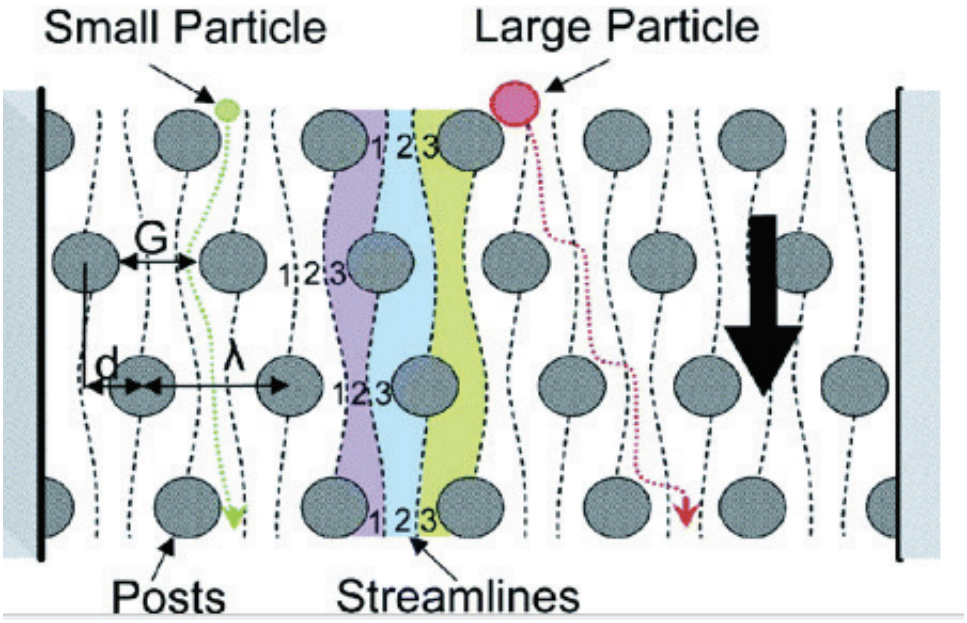

Figure 1.6: Separating large and small particles by dynamic lateral displacement (DLD). [19]

device throughput. [19] Additionally, while DLD chips effectively isolate leukocytes from blood, they commonly suffer from clogging issues leading to shorter operational times and still lower throughput. Furthermore, the trapped CTCs can deform at the pores under constant shear during sample processing, making their retrieval difficult and thus requiring post-sorting analysis to be done on chip.

1.3 Summary

Table 1.1 summarizes the key technologies for cancer cell separation and detection mentioned above. Despite these technological advances, the goal of a single device capable of simultaneously achieving high throughput, high target cancer cell recovery, high purity, and high cell viability remains elusive.

Table 1.1: Existing techniques for isolating CTCs by their biological or physical properties.

Techniques	**Intended to be sensitive to**	**Disadvantages**
Magnetic-based separation	EpCAM level	Non-viability of cells, specificity of biomarkers (low expression of EpCAM level in some cases), low yield
Cell affinity micro-chromatography	EpCAM level	Specificity of biomarkers (low expression of EpCAM level in some cases)
Dielectrophoresis	Cell electrical polarizability	Time consuming, low yield
Filtration	Cell deformability	Cell damage, low throughput
Density gradient centrifugation	Cell density	High g-force, cell-cell interaction, long exposure of cells to chemicals

A significant challenge for cell-affinity micro-chromatography and magnetic activated micro-cell sorting techniques is their low processing throughput. This is limited by the number of sufficient interactions between surface-bound ligands and target cancer cells. Although various capture structures such as microposts, 3D nano-structures, and patterned herringbones have been shown to increase these interactions, current device throughputs remain at only milliliters per hour. [20] While these techniques permit reasonably high cancer cell capture purity by using highly selective antibodies, non-specific absorption of cells onto device surfaces continues to be an obstacle to increased capture purity.

Since DEP techniques leverage differences in both cellular size and dielectric properties, they could potentially lead to a higher cancer cell separation yield and purity compared to micro-filtration methods that are based on cell size differences only. However, in practice, due to the limited dielectric differences between target cells and carrier cells, the yield and purity of DEP-based techniques are low and the viability of cells processed using DEP is a concern.

Filtration methods have a higher throughput since they are compatible with higher flow rates. Micro-filters also enable higher capture purity of CTCs compared to affinity-based techniques due to the significant size and deformability differences between CTCs and blood cells. However, filtration methods suffer from low cell viability resulting from potential damage incurred as cells pass through narrow filter pores, which renders micro-filters less suitable for live cell interrogations.

Chapter 2

Innovation and Impact

Of all the physical properties of cells that could be the used to distinguish circulating tumor cells from healthy blood cells, **cell density** (the mass-to-volume ratio of the cell) is perhaps the most powerful. Previously, we made the first precision measurements of the density of single living cells, and we found that cell types that are indistinguishable by mass or volume can often be distinguished by density. [21] For example, mouse leukemia cells increase in density mere minutes after treatment with a drug that induces apoptosis; this density increase is so clear that **individual cancer cells can be identified as reacting to the drug based solely on their density.**

Circulating tumor cells typically have a different density than other blood cells [22] and thus CTCs can be isolated from blood using density gradient centrifugation as described in the previous chapter. In this technique, when cells placed in a fluid with a density gradient (more dense at the bottom, less dense at the top) and exposed to high g-forces in a centrifuge, the cells will sink or float to the location where the cell's density

is equal to the fluid's density (the cell is neutrally buoyant). But centrifugation also has disadvantages in many applications. As noted above, cell-to-cell interactions can complicate density gradient separations (if two cells of different densities adhere together, they will sink or float to a location that represents the average of their two densities). The lengthy exposures to concentrated chemicals used to construct the density gradient and high g-forces during centrifugation can affect the viability of separated cells. The resolution of density gradient centrifugation is limited by the uniformity of the density gradient. As a "batch" technique, the throughput and possible therapeutic value of the technique are both limited. Finally, centrifuge equipment is bulky and expensive, and transferring samples into and out of a centrifuge adds significant manual labor and cost to the procedure.

Different types of cancers produce CTCs with different characteristics, and currently no single technique can be used to isolate and detect all types of CTCs. Rather, each technique needs to be optimized for a particular cancer type. For example, antibody-antigen bonds in magnetic-based CTC separation devices must be modified depending on the type of cancer to be detected, and CTC separation devices based on size need to be optimized based on the size of the cancer cells of interest.

To address the drawbacks of previous methods and to facilitate high-efficiency capture of CTCs, **we demonstrated a simple passive and label-free gravity-driven microfluidic "density sorter chip" capable of capturing and isolating cell of interest from blood cells based on their densities.** This method has the potential for continuous high-throughput measurement and classification of whole cell populations in a non-destructive manner, so separated cells can be collected for additional analysis.

The proposed technique could continuously sort a stream of cells purely by their densities (without being influenced by their other physical properties) and could isolate CTCs from other blood cells with **higher throughput, higher accuracy, higher resolution, and gentler conditions than existing density-based CTC separation tools.**

Chapter 3

Preliminary studies of multi-density fluid flows

To understand the behavior of fluids with different densities under laminar flow conditions, we created a simple H-shaped channel layout using Tygon lab tubing. Figure 3.1 shows how we were able to precisely control fluid flow inside tubing by merely changing the orientation of the tubing relative to Earth's gravity.

Inlet 1 contains a less-dense yellow fluid and Inlet 2 contains a more-dense blue fluid. When the chip is oriented at 90° relative to gravity, the fluids rotate 90° clockwise to orient the more-dense blue fluid on the bottom of the channel and the less-dense yellow fluid on the top. When the H-channel splits into two outlets, each outlet receives an identical mixture containing 50% yellow fluid and 50% blue fluid. Consequently when the H-channel chip is rotated 0°, the force of gravity causes the fluids to swap places in the horizontal channel, placing the more-dense blue fluid on the bottom of the channel and the less-dense

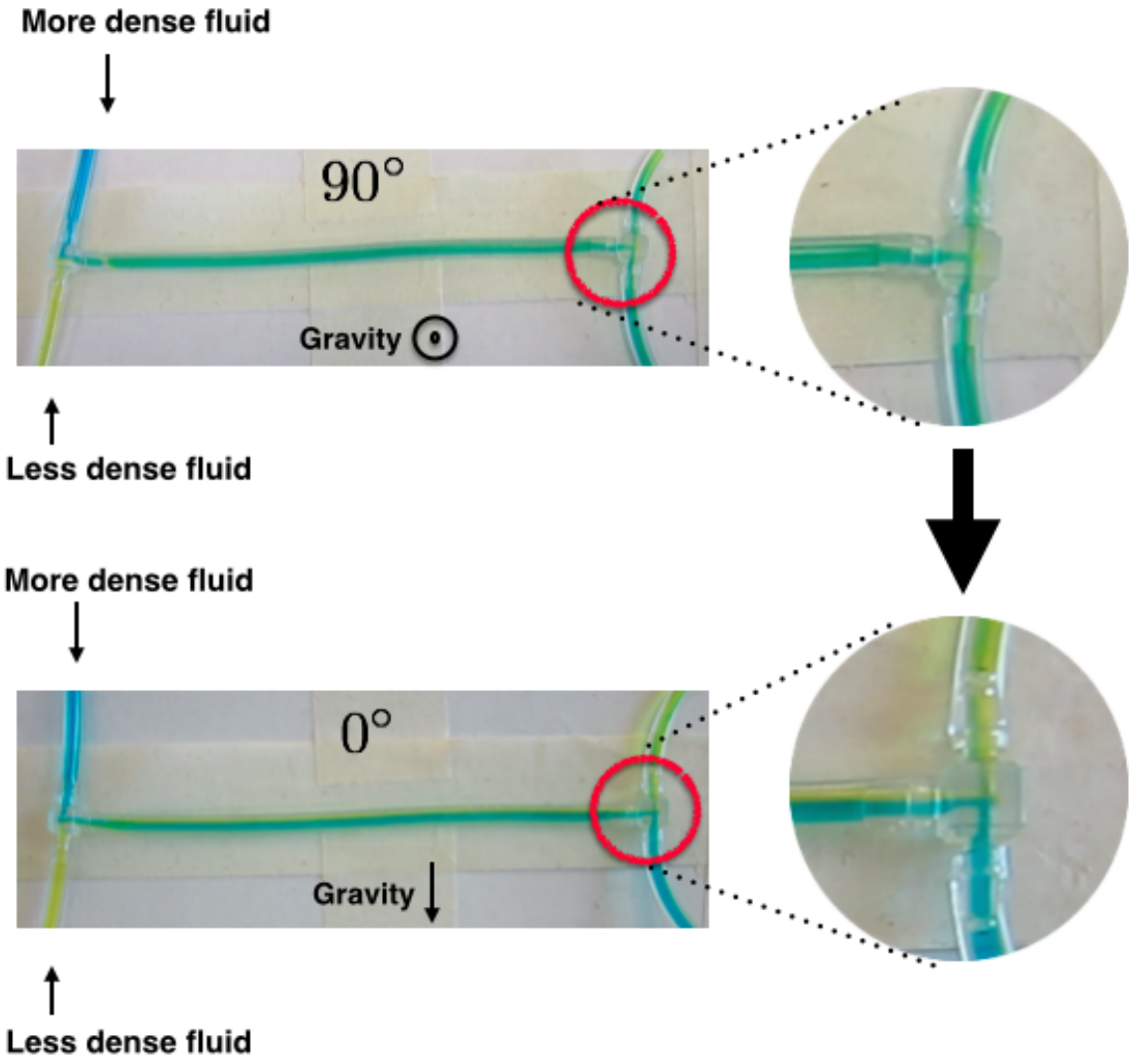

Figure 3.1: Preliminary studies of multiple fluid densities in channel. The mixture of blue and yellow fluid at the two outlets is determined by the angle of the tubing assembly relative to Earth's gravity: a 50:50 mixture in each outlet results when the tubing assembly is orthogonal to gravity, and essentially unmixed blue and yellow fluid results when the assembly is parallel to gravity.

yellow fluid on the top. (Figure 3.1). When two streams of fluid with different densities merge together into a single horizontal microfluidic channel under laminar flow on-chip, the interface between the two fluids quickly reorients itself to be orthogonal to Earth's gravitational force. In this manner, the orientation of a microfluidic chip may be used to route fluids in different directions on-chip without using any off-chip control hardware.

By miniaturizing the density gradient to a micron-scale chip, only 1 g (Earth's gravity) and only a few seconds are required for fluid to change orientation. We used these results as the proof-of-concept for a generic strategy for controlling microfluidic chips based on their orientation (Chapter 5).

Chapter 4

3D printed microfluidics

The results in the previous chapter suggest that chip orientation can be used to control flow in microfluidic devices. To demonstrate this control principle on a real microfluidic chip, we needed to replicate the tubing assembly from Figure 3.1 in a real microfluidic device. We chose to use 3D printing to create this chip because the technology allows for chip designs that would be difficult or impossible to create using traditional (2D) microfabrication.

Commercial 3D printers are not intended for use in printing microfluidic chips, so before we could use our printer to fabricate actual microfluidic chips, we needed to first characterize the performance of our printer. Figure shows a printed test chip containing a range of microfluidic channel widths. This test chip was designed using SolidWorks (Dassault Systèmes, Vélizy-Villacoublay, France), exported as an .STL file, and printed using a 3D printer (Form 1+, Formlabs, Cambridge, MA). The stereolithography-based printer uses a 405 nm Class 1 laser to polymerize a liquid resin into a solid part. The

perforated platform is then lowered very slightly and the process repeats until a complete object has been printed out. The resin used in this study is a combination of methacrylated monomers and oligomers. This printer has very high resolutions and delivers excellent surface quality.

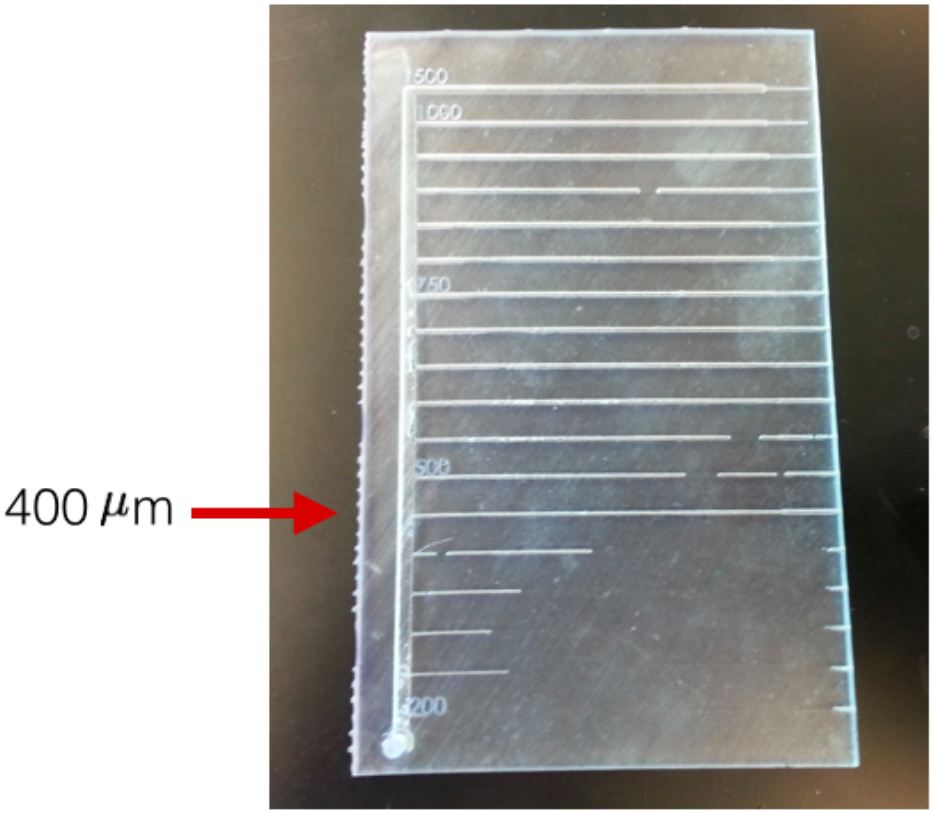

Figure 4.1: 3D printed test fabricated prototype showing different channel widths.

As can be seen, in Figure 4.1, 400 μm is the minimum microfluidic channel diameter that can be successfully printed using our printer.

Based on these results, we designed, printed, and tested a chip-based version of the tubing assembly from Figure 3.1. The chip shown in Figure 4.2 contains a 42 mm long and

1 mm in diameter channel with 3 inlets and 2 outlets. In another advantage of 3D printing, the chip includes barbed tubing connectors that facilitate connection of tubing to the inlets and outlets. This chip is representative of the ones used in exploring orientation-based control of microfluidics in the next chapter.

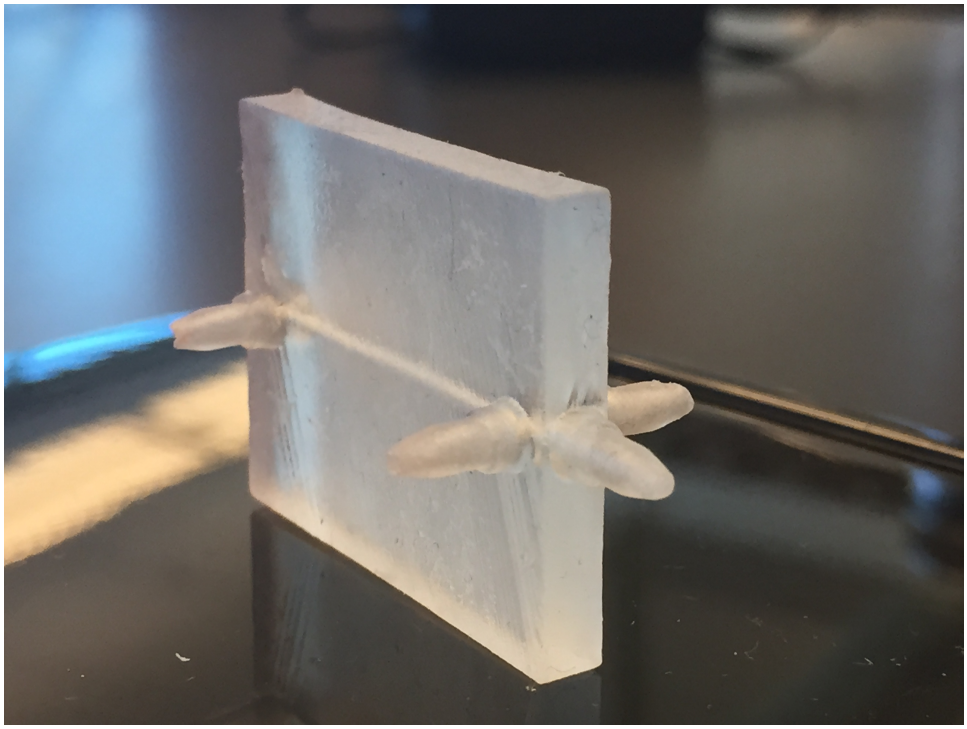

Figure 4.2: A 3D printed microfluidic chip for testing orientation-based control of microfluidics.

Chapter 5

Orientation-based control of microfluidics

Reprinted with permission from Norouzi N, Bhakta HC, and Grover WH (2016), Orientation-Based Control of Microfluidics. PLoS ONE 11(3): e0149259 (2016).

Abstract

Most microfluidic chips utilize off-chip hardware (syringe pumps, computer-controlled solenoid valves, pressure regulators, etc.) to control fluid flow on-chip. This expensive, bulky, and power-consuming hardware severely limits the utility of microfluidic instruments in resource-limited or point-of-care contexts, where the cost, size, and power consumption of the instrument must be limited. In this work, we present a technique for on-chip fluid control that requires no off-chip hardware. We accomplish this by using inert compounds to change the density of one fluid in the chip. If one fluid is made 2% more dense than a sec-

ond fluid, when the fluids flow together under laminar flow the interface between the fluids quickly reorients to be orthogonal to Earth's gravitational force. If the channel containing the fluids then splits into two channels, the amount of each fluid flowing into each channel is precisely determined by the angle of the channels relative to gravity. Thus, any fluid can be routed in any direction and mixed in any desired ratio on-chip simply by holding the chip at a certain angle. This approach allows for sophisticated control of on-chip fluids with no off-chip control hardware, significantly reducing the cost of microfluidic instruments in point-of-care or resource-limited settings.

5.1 Introduction

The advantages of microfluidics over conventional lab-scale techniques—reduced reagent consumption, faster reactions, smaller instrument size, enhanced automation, higher throughput, and so on—have enabled applications for microfluidic instruments in fields as diverse as health care, environmental monitoring, and space exploration. The ability to control fluid flow on a microfluidic chip is a fundamental need in these instruments. However, most existing techniques for controlling on-chip fluid flow rely on off-chip hardware. For example, to control the mixing ratio of two fluids in a microfluidic chip, two off-chip pumps (pressure regulators or syringe pumps) are typically required. Valves and pumps can be moved on-chip [23, 24], but microfluidic valves and pumps also require off-chip hardware (usually computer-controlled solenoid valves and pressure or vacuum pumps). Electrical methods for controlling fluids, such as dielectrophoresis[25, 26] and electrowetting, [27] require off-chip electrical power supplies and complicate the fabrication of the microfluidic

chip. In each of these approaches, the off-chip hardware required to control on-chip fluid flow can *cost thousands of dollars, consume hundreds of watts of electrical power, and contribute significant bulk to the instrument.* Consequently, many microfluidic instruments remain unsuitable for use in point-of-care or resource-limited settings, where instrument cost, power consumption, and size must be minimized.

Here we describe a method for precisely controlling fluid flow inside a microfluidic chip that requires *no off chip hardware.* In this method, by simply orientating a microfluidic chip at a certain angle, on-chip fluids can be routed and mixed in any desired ratios. We accomplish this by adding inert compounds that slightly increase the density of certain fluids in the chip. When two fluids of different densities flow together under laminar flow on-chip, the interface between the two fluids quickly reorients itself to be orthogonal to Earth's gravitational force. If the channel containing the fluids then splits into two channels, the amount of each fluid flowing into each channel is a function of the angle of the channels relative to gravity. In this manner, different amounts of different fluids can be routed on-chip simply by changing the orientation of the microfluidic chip as shown in Figure 5.1.

As a proof-of-concept demonstration, we used the principle of orientation-based microfluidic control in a simple mixer chip that is capable of generating any desired mixing ratio of two fluids. We chose to create a mixer because of the importance of mixing in microfluidic devices. Microfluidic mixers automate the time-consuming process of preparing arbitrary concentrations and mixtures of solutions by hand. Most existing microfluidic mixers utilize either microfluidic valves and pumps [23, 24] or arrays of split-and-combine operations. [28, 29] These mixers have found a variety of uses in microfluidic chips for

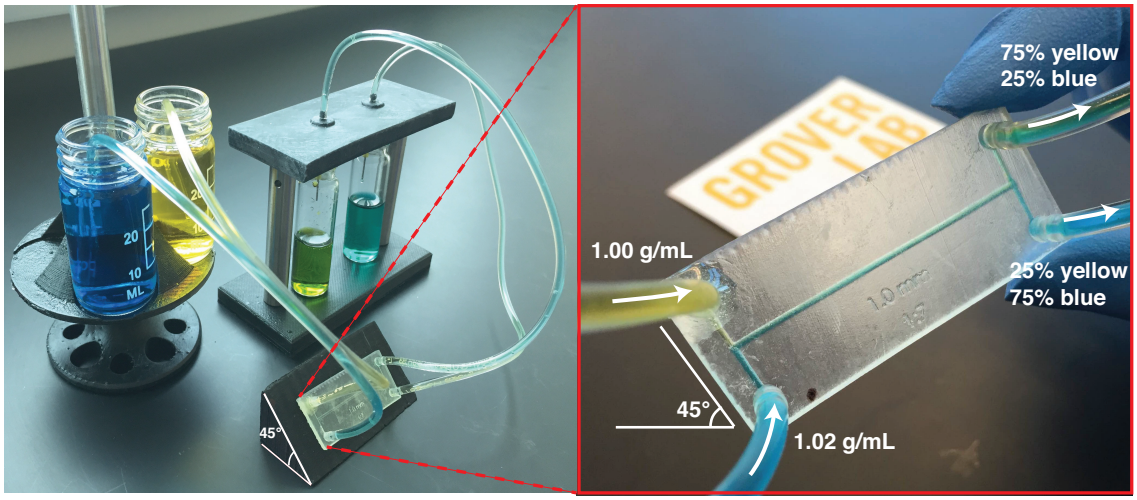

Figure 5.1: Using the orientation of a microfluidic chip to control the mixing ratio of fluids on-chip. Two fluids (yellow and blue) flow into the chip; the blue fluid includes an additive (sucrose) that makes the blue fluid 2% more dense than the yellow fluid. When the two fluids flow together in the chip, the fluids rotate to orient the more-dense blue fluid toward Earth's gravity. When the channel then splits, the amount of each fluid flowing in each direction is precisely controlled by the angle of the chip. By using this approach, any desired mixing ratio of the yellow and blue fluids can be obtained simply by holding the chip at a certain angle; no off-chip control hardware is needed.

evolving novel ribozymes [30], cytotoxicity studies [31], estimation of drug efficiency and optimization of biochemical reactions. [32, 33] However, a chip that uses these existing mixers is capable of generating only certain fixed ratios of mixtures; it cannot be used to generate *any* desired concentration or mixing ratio without redesigning the chip. Additionally, mixers containing microfluidic valves and pumps still rely on off-chip hardware for controlling these valves and pumps. Finally, existing valve- and pump-based or split-and-combine mixers consume a relatively large amount of fluid to generate a relatively small amount of the desired mixture. In summary, there is an unmet need for simple, equipment-free methods for generating arbitrary mixtures of fluids in microfluidic chips.

5.2 Theory of orientation-based microfluidics

To explore the effects of chip orientation on fluid flow inside a microfluidic chip, we used finite element analysis software to simulate the behavior of a simple microfluidic chip held at different angles relative to gravity. Our model combines the Navier-Stokes equations, Fick's law of diffusion, and a function that describes the density of a solution as a function of the concentration of a solute. [34] COMSOL Multiphysics (Burlington, MA) was used to simulate a orientation-controlled mixer chip shown in Figure 5.2. The model simulated the experimental conditions in Figure 5.1: a microfluidic channel with a circular cross section and 1.0 mm diameter, a less-dense yellow fluid with density 1.00 g/mL, and a more-dense blue fluid with density 1.07 g/mL. The fluid phase in the model is governed by

the continuity equation for the incompressible Navier-Stokes equations:

$$\bigtriangledown \cdot u = 0 \tag{5.1}$$

$$\rho u \cdot \bigtriangledown u = - \bigtriangledown P + \rho g + \bigtriangledown \cdot (\mu(\bigtriangledown u + \bigtriangledown u^T)) \tag{5.2}$$

where u is the velocity vector, μ is the fluid viscosity, P is the pressure applied to the upstream end of the fluid, ρ is the density of the fluid, and g is the gravitational acceleration of objects on Earth (9.8 m s^{-2}). The solute concentration follows the equation of conservation of mass and Fick's Law of Diffusion:

$$u \cdot \bigtriangledown c = \bigtriangledown \cdot (D \bigtriangledown c) \tag{5.3}$$

where D is the diffusivity of the solute and c is the concentration of the solute. Equations 5.1–5.3 are coupled through the dependence of a solution's density on its solute concentration, which can be expressed as

$$\rho = \rho_{\text{water}}(1 + Bc) \tag{5.4}$$

where ρ is the density of the solution, ρ_{water} is the density of pure water (1.00 g/mL), c is the solute concentration, and B is an experimentally-obtained, solute-specific constant that correlates a solution's density with its solute concentration (in this study, $B = 127$ L/mol for sucrose). Equations 5.1–5.4 are solved for a steady state flow with inlet solute concentrations of 0 mol/L in Inlet 1 and 1 mol/L in Inlet 2.

The H-shaped microfluidic channel network simulated in 5.2A has two inlets and two outlets. Inlet 1 contains a yellow fluid with density $\rho = 1.00$ g/mL, and Inlet 2 contains a slightly-more-dense blue fluid ($\rho = 1.07$ g/mL). In 5.2A, the chip is oriented such that Inlet 2 is in the same direction as gravity (so the angle θ between Inlet 2 and gravity is

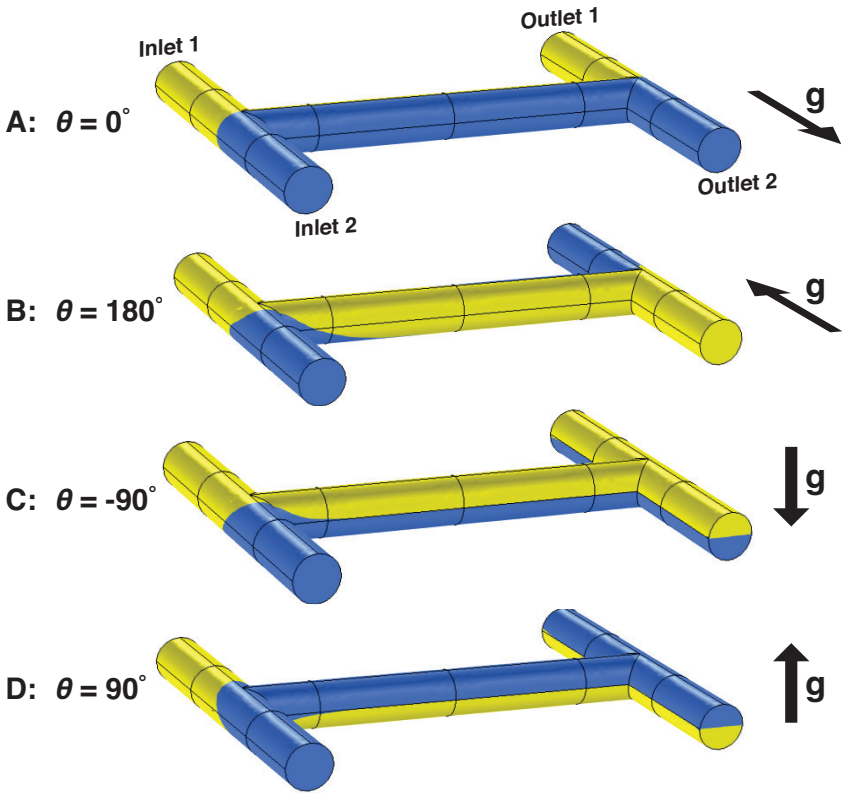

Figure 5.2: Principle of orientation-based control of microfluidics. These simulations show fluid flowing inside a simple microfluidic channel network containing two inlets and two outlets. Inlet 1 contains a less-dense yellow fluid and Inlet 2 contains a more-dense blue fluid. When the chip is oriented such that Inlet 2 is aligned with the Earth's gravitational force **(A)**, the yellow and blue fluids remain unperturbed and exit the chip in the same directions from which they entered (yellow at Outlet 1 and blue at Outlet 2). However, when the chip is rotated 180° **(B)**, the force of gravity causes the fluids to swap places in the horizontal channel, placing the more-dense blue fluid on the bottom of the channel and the less-dense yellow fluid on the top. Consequently, the two fluids exit in the *opposite* directions from which they entered: Outlet 1 contains blue fluid and Outlet 2 contains yellow fluid. When the chip is oriented at $-90°$ relative to gravity **(C)**, the fluids rotate 90° clockwise to orient the more-dense blue fluid on the bottom of the channel and the less-dense yellow fluid on the top. When the channel splits into two outlets, each outlet receives an identical mixture containing 50% yellow fluid and 50% blue fluid. Finally, when the chip is oriented at 90° **(D)**, the fluids rotate 90° *counterclockwise* to once more orient the more-dense blue fluid on the bottom of the channel, and again both outlets contain identical mixtures containing 50% yellow and 50% blue. In this manner, the orientation of a microfluidic chip may be used to route fluids in different directions on-chip without using any off-chip control hardware.

0°). In this orientation, the force of gravity keeps the more-dense blue fluid flowing along the bottom of the channel and the less-dense yellow fluid flowing along the top of the channel. Consequently, when the channel splits into two outlets, the fluids leave in the same directions they came from: the more-dense blue fluid exits through Outlet 2 in the direction of gravity, and the less-dense yellow fluid exits through Outlet 1.

In 5.2B, the chip has been rotated about the middle channel axis by 180°. In this configuration, the force of gravity causes the two fluids to quickly swap places in the middle channel so that the more-dense fluid flows along the bottom of the channel and the less-dense fluid flows along the top. When the channel splits, the fluids exit in the *opposite* direction they came from: the more-dense blue fluid entered from Inlet 2 but exits through Outlet 1, and the less-dense yellow fluid entered from Inlet 1 but exits through Outlet 2. In this manner two different fluids can be routed to two different destinations on-chip by orienting the chip at either 0° relative to gravity (Figure 5.2A) or 180° (Figure 5.2B).

In Figure 5.2C, the chip has been rotated by 90° relative to gravity. The force of gravity again causes the fluids to reorient to place the more-dense blue fluid on the bottom and the less-dense yellow fluid on the top (a clockwise rotation of 90°). When the channel splits, both Outlet 1 and Outlet 2 have the same contents: the bottom-half of each channel is filled with more-dense blue fluid, and the top half of each channel is filled with less-dense yellow fluid. After the contents of each exit channel becomes homogeneous by *e.g.* diffusional mixing, both outlets contain identical mixtures consisting of 50% blue and 50% yellow.

Finally, in Figure 5.2D, the chip has been rotated by -90° relative to gravity. This case is similar to Figure 5.2C; gravity once more causes the two fluids to reorient to place the more-dense blue fluid on the bottom and the less-dense yellow fluid on top (a *counterclockwise* rotation in this case) and the exit channels each contain the same mixture (50% yellow and 50% blue).

The results in Figure 5.2 can be generalized for any angle of orientation θ. If the less-dense fluid at Inlet 1 contains a solute A with a concentration $[A_0]$, and the more-dense fluid at Inlet 2 contains a solute B with concentration $[B_0]$, the concentrations $[A]$ and $[B]$ in each of the outlet channels are:

$$\begin{aligned} [A] &= [A_0]\frac{\theta}{180} & [B] &= [B_0]\left(1-\frac{\theta}{180}\right) & &\text{at Outlet 1} \\ [A] &= [A_0]\left(1-\frac{\theta}{180}\right) & [B] &= [B_0]\frac{\theta}{180} & &\text{at Outlet 2} \end{aligned} \tag{5.5}$$

Using the above equations, we can predict the concentrations [A] and [B] flowing in a chip held at any desired angle θ. These equations only apply to a microfluidic chip with circular cross-section channels, although similar equations may be derived for other channel shapes.

5.3 Materials and Methods

To demonstrate the principle of orientation-based control of fluid flow in a microfluidic chip, we fabricated microfluidic chips similar to the one simulated in Figure 5.2. Microfluidic chips were designed using SolidWorks (Dassault Systèmes, Vélizy-Villacoublay, France), exported as an .STL file, and printed using a 3D printer (Form 1+, Formlabs,

Cambridge, MA). These chips contain a H-shaped microchannel 42 mm long and 1 mm in diameter. The Stereolithography-based printer uses a 405 nm Class 1 laser to polymerize a liquid resin into a solid part. The resin used in this study is a combination of methacrylated monomers and oligomers.

Figure 5.3 shows our test chip in operation. Inlet 1 contains water, density $\rho = 1.00$ g/mL, and Inlet 2 contains more-dense sucrose solution, $\rho = 1.07$ g/mL. Sucrose solutions of precisely known densities were prepared using our software NaCl.py (available for download at http://groverlab.org). FD&C Blue #1 and Yellow #6 were used specifically for visual characterizations. The inlets were connected by tubing to fluid reservoirs that were held 3 cm above the chip. Since the inlet reservoirs were higher than the outlet reservoirs, a head pressure $P = \rho g h$ developed that pumped fluid flow from the input reservoirs through the chip and to the output reservoirs ($g = 9.8$ m s^{-2} and h = height difference between input and output reservoirs). The inlet and outlet reservoirs were maintained at the same height regardless of the tilt of the chip. Consequently, the orientation of the chip does not affect the flow rate. No off-chip fluid control hardware like pumps or valves were used.

The phenomenon of orientation-based control depends upon convection, not diffusion, being dominant in the microfluidic system. A dimensionless parameter called the Peclet number, Pe, is used to determine whether convection or diffusion is dominant in a system:

$$Pe = \frac{Lu}{D} \tag{5.6}$$

where L is the characteristic length, u is the flow velocity, and D is the solute's diffusion coefficient. The calculated Peclet number for our flow rate ($\sim$11,000) is much greater than

one, indicating that convection is dominant and diffusional mixing between the different fluid streams is negligible.

Chips of different channel geometries were held at different angles. The average residence time of fluid in the chip was calculated to be 0.7 seconds. To make sure that the system reaches steady state, samples were collected from the chip after 1 minute of flow. Samples of 5 mL were collected from each outlet for each orientation and chip geometry. To quantify the resulting mixing ratios, fluids from both outlets were collected and analyzed using an UV-Vis-NIR spectrophotometer (V-670, Jasco, Easton, MD).

5.4 Experimental Results

When the chip is oriented on its edge relative to gravity in Figure 5.3A ($\theta = 0°$), the more-dense blue fluid remains on the bottom of the horizontal channel and the less-dense yellow fluid remains on the top of the channel. Consequently, the fluids exit the mixer chip in the same directions from which they entered (yellow fluid at Outlet 1 and blue fluid at Outlet 2). This case is identical to the simulation shown in Figure 5.2A. When the chip is held flat relative to gravity in Figure 16B ($\theta = 90°$), the two fluids reorient relative to gravity (rotating 90° clockwise) to place the more-dense blue fluid at the bottom of the horizontal channel and the less-dense yellow fluid on the top of the channel. When the horizontal channel splits, both output channels have the same contents ($\sim 50\%$ yellow and $\sim 50\%$ blue, which appears as green in the outlets). This situation is identical to the simulation shown in Figure 5.3C. Finally, when the chip is oriented on its *other* edge in Figure5.3 C($\theta = 180°$), the yellow and blue fluids swap places in the horizontal channel to

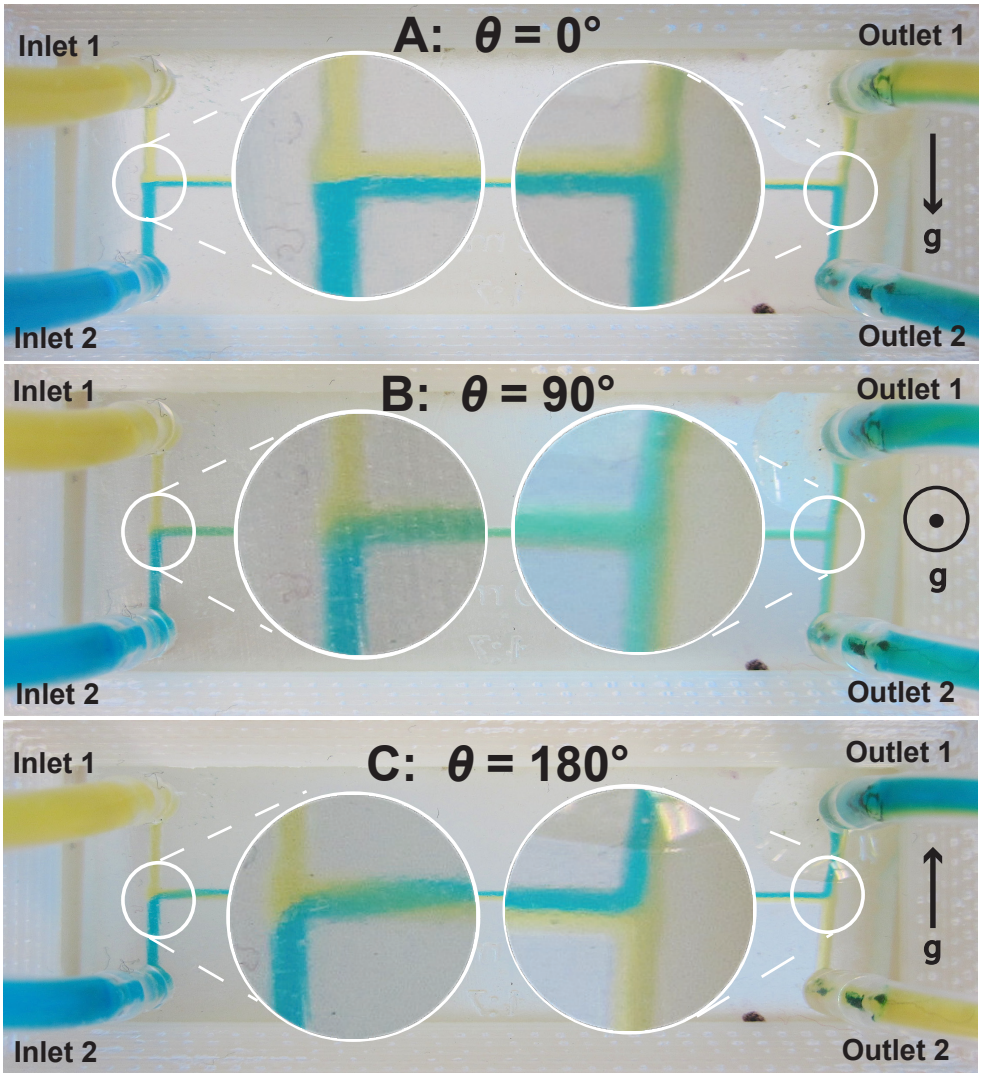

Figure 5.3: Photographs of a microfluidic mixer chip oriented at different angles θ relative to gravity. In each case Inlet 1 contains a less-dense yellow fluid (water; density $\rho = 1.00$ g/mL) and Inlet 2 contains a more-dense blue fluid (sucrose solution; $\rho = 1.07$ g/mL). When $\theta = 0°$ **(A)** the arrangement of yellow and blue fluids in the horizontal channel remains unchanged, and Outlet 1 contains yellow fluid and Outlet 2 contains blue fluid. However, at $\theta = 90°$ **(B)** gravity causes the more-dense blue fluid to move to the bottom of the horizontal channel and the less-dense yellow fluid to move to the top. This twists the contents of the horizontal channel by 90° and causes both outlets to contain identical mixtures containing $\sim 50\%$ blue and $\sim 50\%$ yellow. Finally, at $\theta = 180°$ **(C)** the gravity-induced repositioning of the fluids in the horizontal channel causes the fluids to twist by 180°, effectively swapping places in the channel. As a result, the two fluids exit the chip in directions *opposite* from where they entered, with Outlet 1 containing blue fluid and Outlet 2 containing yellow fluid.

place the more-dense blue fluid on the bottom and the less-dense yellow fluid on the top. Consequently, the fluids leave the Outlet channels *opposite* from where they entered, with yellow fluid at Outlet 2 and blue fluid at Outlet 1.

To demonstrate orientation-based control of fluid flow over a wide range of angles (not just the three angles shown in Figure 5.3), the mixer chip was operated at angles from 0° to 180° in 15° increments. As before, the more-dense blue fluid was a sucrose solution (density = 1.07 g/mL) and the less-dense yellow fluid was water (density = 1.00 g/mL). Figure 5.4 shows the concentration of each dye in the two output channels. As the mixer chip's angle of rotation θ is varied from 0° to 180°, the concentration of blue fluid rises and yellow fluid drops in Outlet 1, and an opposite trend is observed in Outlet 2. The relationship of concentration on angle of rotation is roughly linear as predicted by Equation 5.5. This experimental data deviates from the predicted model at angles near 0° and 180°, where the outlet fluids concentrations are not 100% and 0% as predicted but ∼90% and ∼10% instead. This is likely due to diffusion within the horizontal channel in the mixer chip, which contributes a small amount of mixing between the two fluid streams. The effect of this diffusional mixing is most pronounced at angles near 0° and 180° where the outlets should contain pure (unmixed) fluids according to Equation 5.5; instead their contents are ∼90% pure. Additionally, the relationship of fluid concentration on angle of rotation in Figure 5.4 is not purely linear but appears to have some higher-order shape. This can be attributed to the cross-sectional geometry of the 3D-printed microfluidic channel because of the limited resolution of the 3D printer. The 1 mm channel was printed using a stereolithography 3D printer with a tolerance of ± 200 μm. This could result in a microfluidic channel that is

not perfectly circular and requires a more complex model than the one shown in Equation 5.5. However, the error bars in Figure 5.4 confirm that the outlet concentrations are a reproducible and predictable function of the angle of rotation of the chip, and a higher-order function could easily be derived that predicts the fluid concentrations in a chip at any rotation angle θ to within a few percentage points.

To explore the role of channel cross-section shape in orientation-controlled microfluidics, we designed and 3D printed mixer chips with square (1×1 mm) and rectangular (1×1.25 mm). Figure 5.5A confirm that the orientation of a chip can still be used to control fluid mixing in chips with square and rectangular cross sections, though increased deviation from the predicted fluid concentrations is observed in the rectangular cross-section chip. This suggests that orientation-based control of microfluidics works best in channels with aspect ratios near one; at higher aspect ratios the channel geometry hinders the desired rotation of fluid in the channel. We were limited to a 1 mm channel diameter since we wanted to explore different geometries and aspect ratios using a 3D printer; however, the same phenomena were observed in a conventional glass microfluidic channel of 180 μm (data not shown). We also examined the behavior of two fluids of different densities flowing in rectangular channels with much higher aspect ratios (cross-sectional dimensions 1 mm $\times$ 5 mm; data not shown). The experimental results further support the assertion that orientation-based control of microfluidics is most practical in channels with cross-sectional aspect ratios near one (circular and square channels).

In addition to channel geometry, fluid density has an effect on our phenomenon. The speed at which rotation occurs is influenced by the density difference. However, in

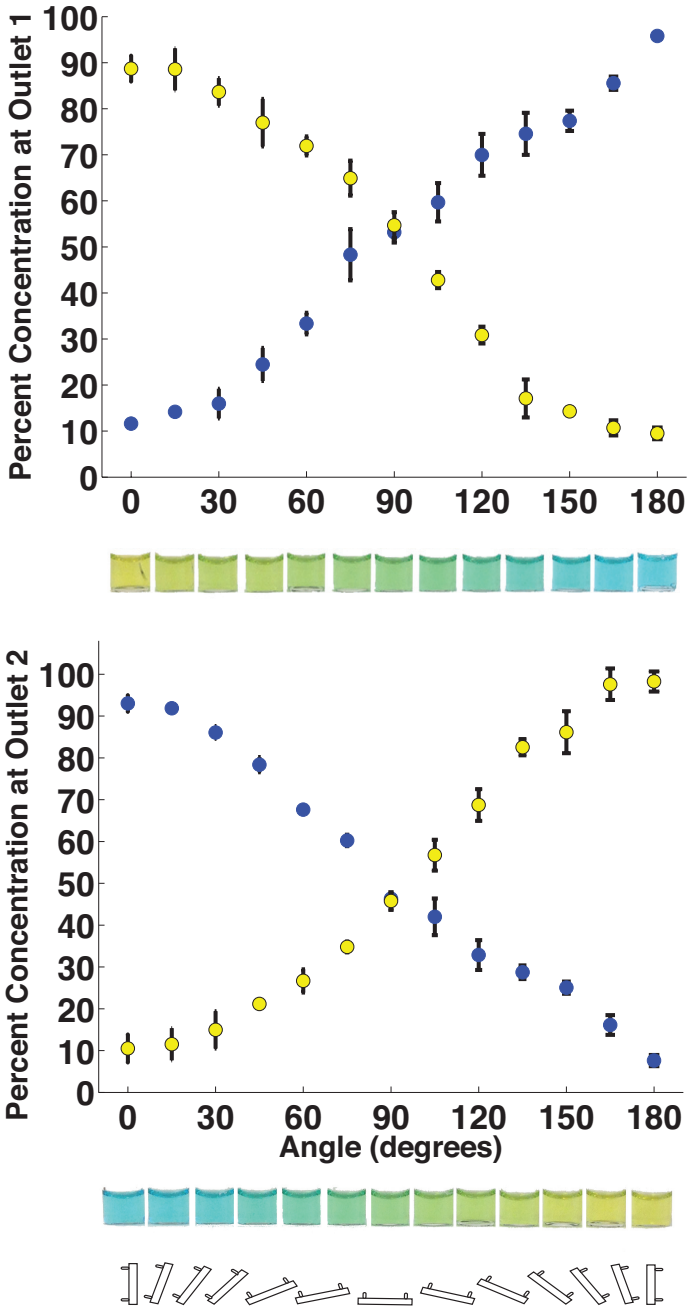

Figure 5.4: Concentrations of yellow and blue dyes in the mixer chip's two outlets as the angle of rotation of the mixer chip is varied from 0° to 180°. Also shown are photographs of the fluid collected at each outlet and an illustration of the chip's orientation at each angle of rotation. $N = 3$ measurements for each point; error bars indicate ± 1 standard deviation. These results show that mixture composition is a function of the angle of rotation of the chip, and any desired mixture can be generated simply by orienting the chip and the required angle.

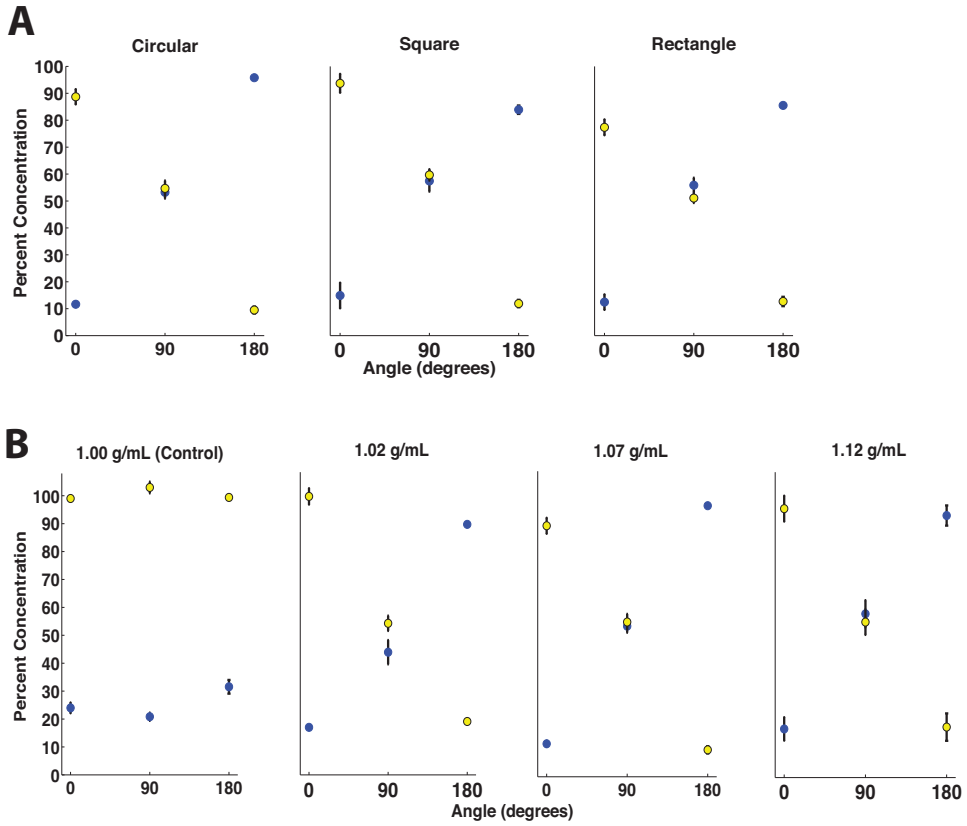

Figure 5.5: **(A)** Concentrations of yellow and blue dyes at Outlet 1 in mixer chips held at 0°, 90° and 180°, for chips with circular, square, and rectangular channel cross-sections. Chip orientation can be used to control on-chip fluids in devices with a variety of channel cross-sectional shapes, although performance deteriorates somewhat in the rectangular channel. These results suggest that microfluidic channels with aspect ratios close to one are best suited for orientation-based control. **(B)** Outlet fluid concentrations measured at Outlet 1 while orienting the mixer chip at 0°, 90° and 180° for four different fluid densities at Inlet 1. The density of fluid at Inlet 2 was kept constant at 1.00 g/mL. When there is no difference in fluid densities between the two inlet fluids, fluid reorientation is not observed and orientation-based control cannot be used (Control case). However, if the fluid density in Inlet 1 is just 2% greater than the fluid density in Inlet 2, then the flowing fluids reorient with respect to gravity and orientation-based control is possible.

practice we found that all rotations we observed were nearly instantaneous. The channel length was kept excessively long for characterization purposes. However, for a channel diameter of 1 mm, a minimum length of 10 mm is required for the rotation to occur. The larger the difference between fluid densities, the quicker the rotation occurs. Rotation speed could be increased by further increasing the difference between fluid densities; however, the resulting increase in concentration gradients will result in an increase in diffusive flux, potentially allowing for more mixing between the two layers.

To determine how much of a difference in density between the two fluids is necessary to employ orientation-based control, sucrose solutions with different concentrations (and thus different densities) were prepared as shown in Figure 5.5B. Experiments were performed using solutions with densities of 1.00 g/mL (control), 1.02 g/mL, 1.07 g/mL, and 1.12 g/mL. As before, the density of the second fluid was kept constant at 1.00 g/mL (water). In the control case in Figure 5.5B, there is no difference in densities between the two fluids in the mixer chip, so no reorientation of the fluids occur within the chip and the fluid concentrations at the outlets are constant regardless of the angle of orientation of the chip; however, when the density of one input fluid is increased by only 2% to 1.02 g/mL, the fluids again reorient with respect to gravity and orientation-based control is demonstrated.

5.5 Conclusions

We demonstrated that the orientation of a microfluidic chip can be used to precisely control the flow of fluids inside the chip. By using the orientation of a chip to control fluid flow instead of on-chip valves or off-chip pumps and regulators, our technique can eliminate

a substantial portion of the cost, size, and power-consumption of a microfluidic assay or instrument. Thus, this technique should facilitate the spread of microfluidic technologies to new applications in resource-limited and point-of-care settings.

Orientation-based control of microfluidics does depend upon different fluids in the chip having different densities. However, the amount of density difference necessary to use orientation-based control is very small (only $\sim$2%), and there are many different substances that can be added to a fluid to adjust its density. For applications that do not require precise control of the osmotic strength of fluids, small amounts of solutes like sucrose (as used here) and sodium chloride can be easily and inexpensively added to a fluid to enable orientation-based control. For applications in which the osmotic strength of the fluid *does* need to be controlled, a number of compounds have been developed that increase a fluid's density without affecting its osmotic strength. These include Ficoll, a high molecular weight polysaccharide used in density gradient centrifugation [35]; Percoll, a colloidal silica solution which is biologically inert and also used in density gradient centrifugation [36]; Visipaque, an isotonic, nonionic, nontoxic compound used as an intravenous contrast agent in radiography [37] and metatungstate solutions, a dense, inert and inorganic solutions with low reactivity. By adding small amounts of substances like these to fluids and using the principle of orientation-based control, microfluidic assays can run with little or no off-chip hardware.

A density difference of $\sim$2% is required for fluid reorientation to occur. Increasing the density of a solution by $\sim$2% may change the viscosity of the solution. For example, increasing the density of a sucrose solution by 2% increases the effective viscosity of the

solution by 17%. However, this viscosity difference is actually too low to affect the concentration of the output fluid. Karst *et al.* [12] studied fluids of different viscosities flowing alongside each other in laminar flow (as is the case in the horizontal channel of our chip). They found that the ratio of the volumes occupied by each fluid inside the tube is not equal to the ratio of the fluids' flow rates. Moreover, they found that the viscosity of the second fluid has to be at least 100% greater than the viscosity of the first fluid for the ratio of the volumes of the two fluids in the channel to be altered. Therefore, the effect of fluid viscosity is minimal.

Finally, is orientation-based control powerful enough to control real-world microfluidic chips. Certainly chips with hundreds of computer-controlled valves offer a level of fluid control that may be unattainable by orientation-based control (though this level of control comes with a significant cost). However, many real-world microfluidic devices require simpler fluid control and could be controlled using chip orientation. For example, the proof-of-concept mixer chip shown here could be used in a drug toxicity screening assay by exposing cells downstream of the mixer to various concentrations of a drug. [38] This could be accomplished by flowing a drug solution in one inlet and a diluent with 2% greater density in the second inlet, and trapping cells in one of the outlet channels. By orienting the chip at a certain angle and then assessing the viability of the cells, the response of the cells to a particular concentration of the drug could be assessed. Assuming that a chip can be held at an angle with an accuracy of ± 5 degrees, the resulting drug concentration should be accurate to about $\pm 10\%$ which is adequate precision for many drug screening asays. This is one of many real-world microfluidic assays and diagnostics that could be performed with

little or no off-chip control hardware using orientation-based control.

Chapter 6

Additional technical work in support of "orientation-based control of microfluidics"

6.1 Using an Arduino microcontroller to automate orientation-based control of microfluidics

To demonstrate the automated version of principle of orientation-based control of fluid flow in a microfluidic chip, we created a 3D-printed pivoting platform controlled by a servo connected to a Arduino microcontroller. The microfluidic chip from the previous chapter is housed within the platform and can be oriented at any desired angle relative to gravity as shown in Figure 6.1.

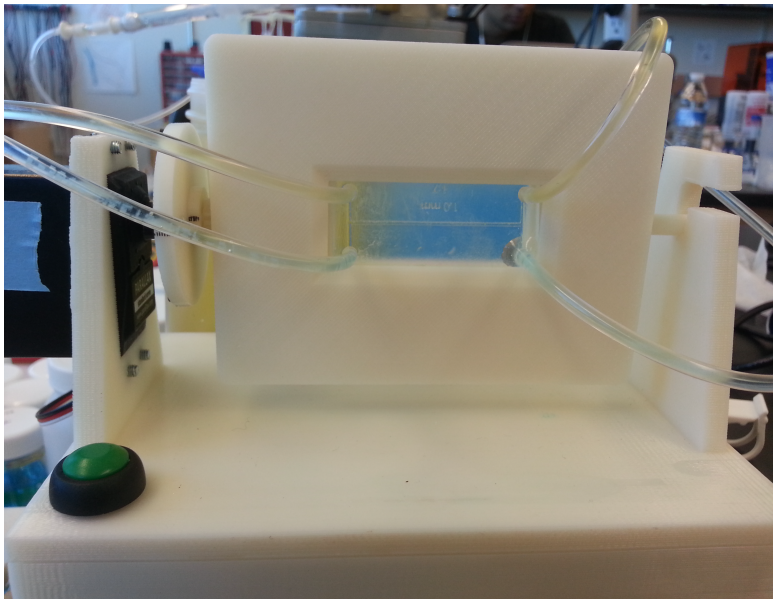

Figure 6.1: 3D printed mixer chip mounted in the center of a rotating stage. The Arduino-controlled stage is capable of orienting the chip at any desired rotational angle relative to gravity.

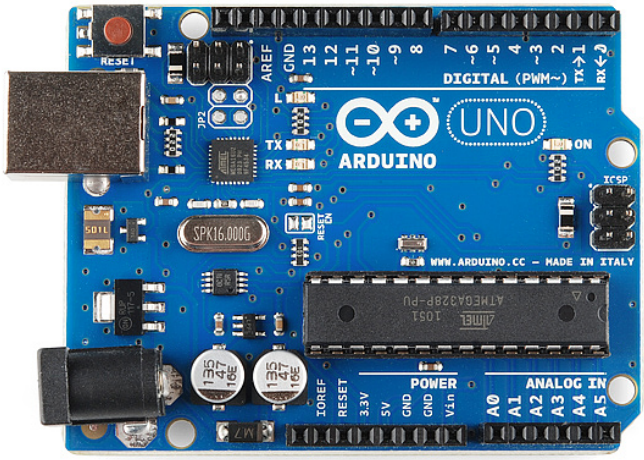

Figure 6.2: Arduino circuit board.

The Arduino is an open-source platform used for building electronic projects; it consists of both a physical circuit board (often referred to as a microcontroller) and a piece of software or IDE (Integrated Development Environment) that runs on a computer and is used to write and upload computer code to the physical board using a USB cable. The servo rotates the stage which holds the mixer chip at angles from 0° to 180° for a total of 13 different angles in order to generate different solute concentrations ratios. The Python code used to control the servo via the Arduino is reprinted in the Appendix.

6.2 Using a simple protractor in orientation-based control of microfluidics

Figure 6.3 shows how it is also possible to use a simple protractor to orient the microfluidic chip and thereby control fluid mixing on-chip. As before, all inlet and outlet fluidic connections to the mixer chip used 3.2 mm/1.6 mm (outer/inner diameter) Tygon tubing (Cole-Parmer). Tubes connected to inlets were placed in their respective input reservoirs. Both input reservoirs were kept at the same height initially in an elevated position and the device was filled with both solutions of different densities by applying a vacuum to the outlet tubes. Once a constant rate of fluid flow was achieved in each outlet, the vacuum was removed. Since the input reservoirs were slightly higher than the outlet reservoirs, a head pressure $P = \rho g h$ developed that continued to drive fluid flow from the input reservoirs through the chip and to the output reservoirs (ρ = fluid density, g = 9.8 m s^{-2}, and h = height difference between input and output reservoirs). This is an efficient and inexpensive way to implement pumping without using expensive syringe

pumps, complicated electrical connections, or active mechanical valves.

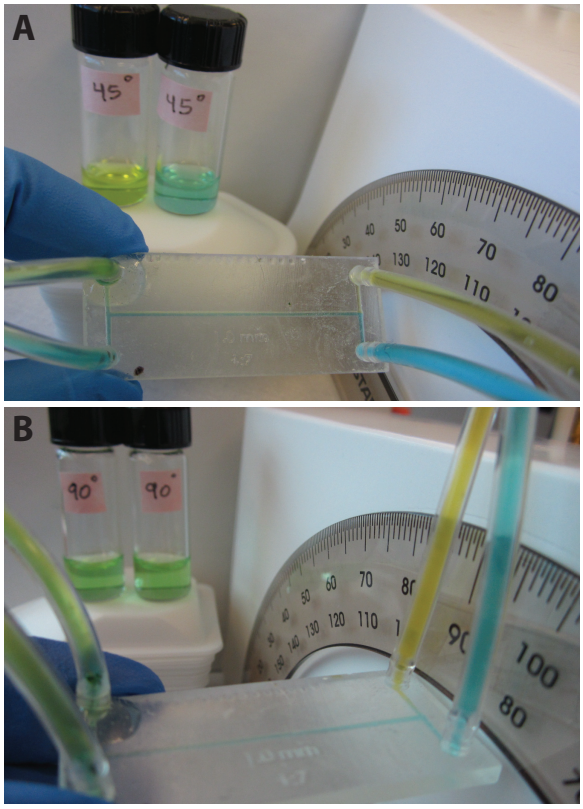

Figure 6.3: Mixer chip generating fixed concentration ratios by orienting the chip at **A)** 45° and **B)** 90° using a simple protractor.

Chapter 7

Applying Stokes' law to cells flowing in our microfluidic chips

Based on our results in previous chapters, we realized that our multi-density fluids under laminar flow could be used as a continuously-flowing density gradient to separate cells and other samples by their densities. In this chapter we explain how our 3D printed microfluidic "density sorter chip" chip has the capability of extracting specific cells or particles from a sample based solely on the density of the cell or particle. Proof-of-concept experiments of this technique (using it to sort microbeads based on their polymer composition and blood cells based on their type) are the subject of the next chapter.

When two fluids of different densities flow together under laminar flow in the microfluidic chips described in the previous chapters, a sharp interface forms between the two fluids. If cells (or other samples of interest) are added to this interface, the cells that are more dense than the lower fluid leave the interface and sink slightly into the lower

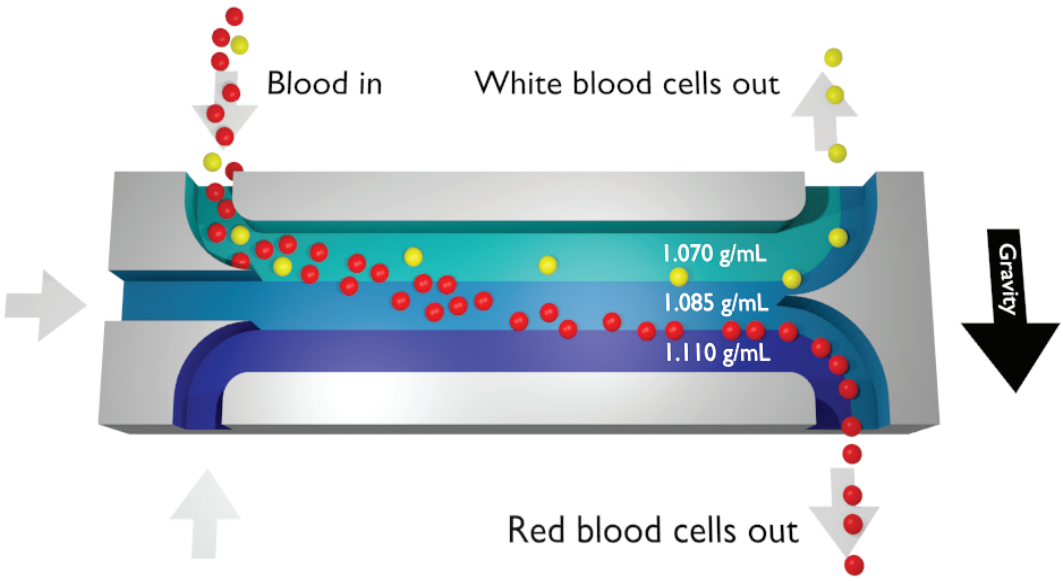

Figure 7.1: Prototypes density sorter chip used to confirm that the density bilayer is stable over various flow conditions. Three inlets device with three different fluid densities and sample flowing from middle inlet.

fluid. Additionally, cells that are less dense than the upper fluid leave the interface and float slightly into the upper fluid. At its end, the horizontal channel splits into two exit channels that receive cells with densities in the desired range. Cells with lower densities exit via the upper channel, and cells with higher densities exit via the lower channel, as shown in Figure 7.1. Cells in these fractions can then be collected for enumeration, additional studies, or even possible transfusion of CTC-free fractions of blood cells back into a patient for therapeutic uses.

As cells flow along the density bilayer, the cells whose density is outside of the selected range have enough time to sink or float into the top or bottom fluid streams. Stokes' law allows us to calculate the velocity at which a cell sinks down or floats up in a fluid:

$$\nu = \frac{2}{9}\frac{\rho_c - \rho_f}{\mu} g r^2 \tag{7.1}$$

where ρ_c is the density of cell, ρ_f is the density of the fluid, μ is the viscosity of the fluid, g is the gravitational acceleration and r the radius of the cell . To derive Stokes' law we first need to draw a free body diagram (FBD) of the sphere including all of the internal and external forces acting on the sphere as it is dropped into the fluid as shown in Figure 7.2. The FBD lists three forces acting on the sphere; F_b, F_d, and F_g. The first two forces arise from the buoyancy effect of displacing the fluid and from the viscous drag of the fluid on the sphere, respectively. Both forces act upwards, buoyancy tending to "float" the sphere (F_b) and the drag force of the fluid on the sphere (F_d) resisting the acceleration of gravity: $F_d = 6\pi\mu V r$, where μ is the fluid viscosity, V is the velocity of the sphere relative to the fluid, and r is the diameter of the sphere. The only force acting downwards is the body force

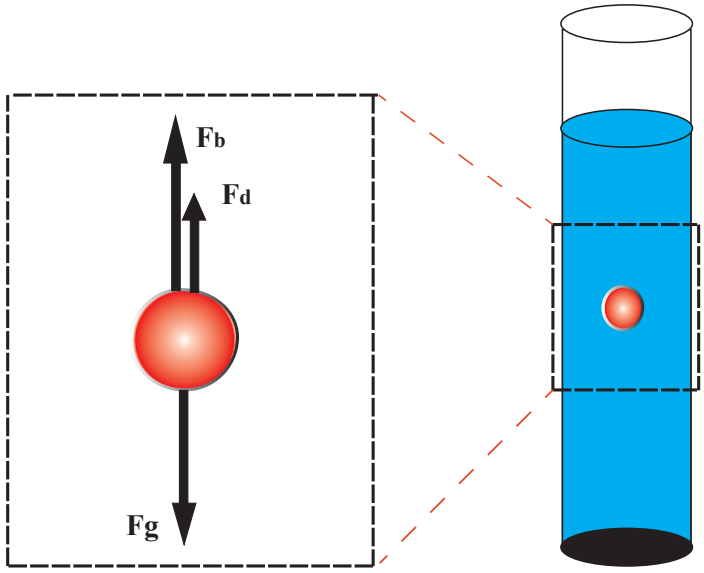

Figure 7.2: Free-body diagram of a sphere in a fluid.

resulting from gravitational attraction (F_g). By summing forces in the vertical direction we can write the following equation:

$$F_b + F_d = F_g \tag{7.2}$$

The buoyancy force is simply the weight of displaced fluid. Combining volume of a sphere (v_{sphere}) with the mass density of the fluid, ρ, the buoyancy force can be written as the product:

$$F_b = F_g = \frac{4}{3}\pi r^3 \rho g \tag{7.3}$$

where g is the gravitational acceleration and r is the radius of the sphere. By combining all of the previous relationships that describe the forces acting on the sphere in a fluid the following expression can be written:

$$\frac{4}{3}\pi r^3 \rho_{\text{fluid}} g + 6\pi\mu V r = \frac{4}{3}\pi r^3 \rho_{\text{cell}} g \tag{7.4}$$

Rearranging and regrouping the terms from the above equation we arrive at the following relationship:

$$\nu = \frac{2}{9}\frac{\rho_c - \rho_f}{\mu} g r^2 \tag{7.5}$$

While Stokes' Law is straightforward, it is subject to some limitations. Specifically, this relationship is valid only for laminar flow. Laminar flow is defined as a condition where fluid particles move along in smooth paths in lamina (fluid layers gliding over one another).

The rate at which a cell rises or falls in fluid is a function of not only the density of the cell (ρ_c) but also the density of the fluid (ρ_f), the viscosity of the fluid (μ), the gravitational acceleration (g), and the radius of the cell (r). For a CTC with reasonable density ($\rho_c = 1.05$ g/mL) and size ($r = 20$ μm) in the density bilayer atop an aqueous fluid with slightly lower density ($\rho_f = 1.04$ g/mL), Stokes' law predicts the cell will drop at 8 μm/s. A spherical cell only has to drop a distance equal to its radius to have its center of mass move into the lower fluid stream, so this CTC would leave the density bilayer and enter the lower stream in just 2.5 s. A smaller ($r = 10$ μm) but otherwise identical CTC would drop slower (2 μm/s), but since it only has to travel 10 μm to enter the lower fluid stream, it would enter the lower stream in just 5 s. These calculations show that as long as the flow rate through the device is slow enough to give the smallest cell of interest enough time to leave the density bilayer, then all larger cells will also have enough time to leave the density bilayer. In other words, above a user-specified cell size threshold, the proposed device is truly sensitive to cell density alone, and the amount of time each cell must spend flowing along the density bilayer is very reasonable (just a few seconds). Since thousands of cells could be flowing along the density bilayer at any given moment, the throughput of

the device could easily be hundreds of cells per second, and by arranging these channels in parallel, tens of thousands of cells could be sorted by their density every second. We demonstrate this in the next chapter.

Chapter 8

Sorting cells by their densities

8.1 Abstract

The ability to sort cells by their type is an important capability in biological research and medical diagnostics. However, most cell sorting techniques rely on labels, which may have limited availability and specificity. Sorting different cell types by their different physical properties is an attractive alternative to labels because all cells intrinsically have these physical properties. But for some physical properties like cell size, the relatively large cell-to-cell variation in cell size within a cell type can make it difficult to identify and sort cells based on their size. In this work we sort different cells types by their density, a physical property with much lower cell-to-cell variation within a cell type (and therefore greater potential to discriminate different cell types) than other physical properties. We accomplish this using a 3D-printed microfluidic chip containing a flowing micron-scale density gradient. Earth's gravity makes each cell in the gradient quickly float or sink to the point where the cell's density matches the surrounding fluid's density, after which the cells are routed

to different outlets and therefore sorted by their density. As a proof of concept, we use our density sorter chip to sort polymer microbeads by their material (polyethylene and polystyrene) and blood cells by their type (white blood cells and red blood cells). The simplicity, resolution, and throughput of this technique make it suitable for isolating even rare cell types in complex biological samples, in a wide variety of different research and clinical applications.

8.2 Introduction

Biological and clinical samples are often heterogeneous populations of many different types of cells. Blood, for example, is a complex mixture of different cell types, only one of which may be needed for a given application [39]. As a result, the ability to separate and sort cells by their type is fundamentally important in modern biological research and medical diagnostics.

Most existing cell sorting techniques can only be applied to certain types of cells. For example, fluorescence-activated cell sorting (FACS) and magnetically-activated cell sorting (MACS) rely on labels or tags that are intended to interact with certain cell types; these techniques cannot be used with cells that lack appropriate labels or tags. And even if, for example, an antibody specific to a particular cell type does exist, antibodies add significant cost to a procedure and complicate the translation of a sorting technique to clinical settings [40].

Label-free techniques for cell separation and sorting can potentially be applied to a much wider range of cell types. For example, filtration [15], cell-affinity micro-

chromatography [15, 16, 17], and dielectrophoresis [18] usually rely on differences in the fundamental physical properties of the cells to be sorted. Since all cells have physical properties like size and deformability, these techniques can theoretically be used to sort a much wider variety of cells than label-based techniques. However, for some physical properties, the intrinsic cell-to-cell variation of that property within a cell type may confound efforts to identify different cells by that property. For example, in human red blood cells (erythrocytes), the coefficient of variation in cell size is called *red cell distribution width* and is typically 11-15% [41]; while this variation has interesting clinical applications [42], it complicates attempts to distinguish red blood cells from other cells based on their size alone.

Of all the physical properties of cells that could be used to distinguish and separate cells of interest, *cell density*—the mass-to-volume ratio of a cell—is perhaps the most powerful. In some cases, cell types that are indistinguishable by sizes (mass or volume) can be distinguished by their density. For example, mouse leukemia cells undergo an increase in density mere minutes after treatment with a drug that induces apoptosis; this density increase is so clear that individual cancer cells can be identified as reacting to the drug based solely on their density, even though the mass and volume of the cells remain virtually unchanged [21].

The conventional tool for separating different cell types by their densities is the *density gradient*. In this almost-eighty-year-old technique, cells are placed in a fluid that contains a range of densities (more dense at the bottom, less dense at the top). The cells then sink or float to the location where the cell's density is equal to the surrounding fluid's

density (this is called the the cell's *isopycnic point*, the location in the density gradient where the cell is neutrally buoyant). Bands containing cells of interest can then be retrieved from the gradient using a pipet.

While density gradients are powerful tools, a number of disadvantages severely limit their utility. First, the buoyant forces that move a cell to its isopycnic point in a density gradient are inherently weak. For a 20 μm diameter spherical cell with a density that is 1% greater than the surrounding fluid density, the Earth's gravitational acceleration (1 g) will pull the cell to its isopycnic point at a velocity of about 2 μm/s or 7 mm/h. This cell would take several hours to travel to its isopycnic point in a centimeter-sized density gradient. In practice, this process can be accelerated by placing the gradient in a centrifuge and applying hundreds or thousands of g's of acceleration (this is the basis for *density gradient centrifugation*). However, prolonged exposure to high g-forces can damage cells by e.g. forcing subcellular components out of the cells [43], and prolonged exposure to the concentrated solutions used to construct the density gradient can affect cell viability [44]. Additionally, the resolution of the technique is limited by the quality of the density gradient [45]. Constructing a smooth gradient of fluid densities that spans several centimeters is challenging, and inconsistencies in the density gradient lead to poor quality cell separation. Also, in density gradient centrifugation, dynamic range and resolution are mutually exclusive. A gradient that spans a wide range of densities can separate a wide range of cells by their densities but cannot discriminate small differences in cell densities; conversely, a gradient that spans a small range of densities can discriminate cells with small density differences but only over a narrow range of densities. Cell-to-cell interactions

can also complicate density gradient separations: if two cells of different densities adhere together, they will sink or float to a location that represents an average of their two densities [46]. Manually retrieving cells of interest from the gradient is a laborious process that can affect the purity of the selected fraction of cells [47]. Moreover, as a "batch" technique, the throughput of density gradient centrifugation is limited to the capacity of a centrifuge tube. Finally, the cost and size of ultracentrifuges used for density gradient centrifugation also limits the utility of the technique in resource-limited settings.

In this work, we demonstrate a simple 3D-printed microfluidic chip that is capable of continuously sorting cells (and other samples) by their densities and can therefore replace density gradient centrifugation in many applications. The chip shown in Figure 1 contains several fluids with different densities. When these fluids flow together under laminar flow conditions, the fluids form what is effectively a micron-scale, continuously flowing density gradient. In this miniaturized density gradient, cells have a very short distance to travel before they reach their isopycnic point, and they travel this micron-scale distance in just a few seconds under the Earth's 1 g of gravitational acceleration (no centrifuge is needed). When the channel then splits, cells with different densities collect in different outlets, ready for enumeration or further analysis. This technique can continuously sort a stream of cells by their densities alone (without being influenced by the cells' other physical properties) and can isolate cell of interest from other cells with higher throughput and gentler conditions than existing tools.

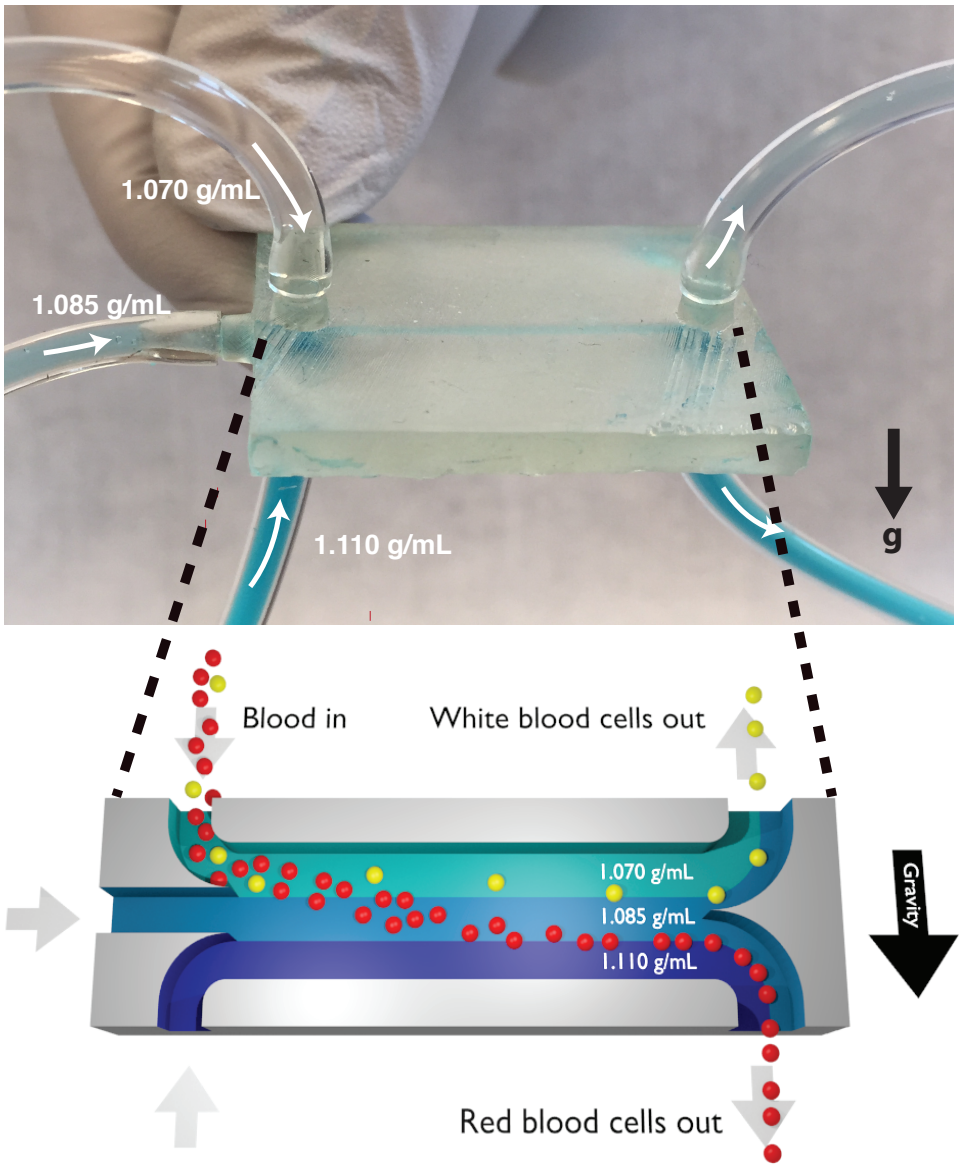

Figure 8.1: Photograph (A) and cross-section illustration (B) of a 3D-printed density sorter chip. Fluids with three different densities (1.070, 1.085, and 1.110 g/mL) are pumped into the inlets; under laminar flow conditions these fluids form a micron-scale density gradient flowing along the horizontal channel. If a mixture of blood cells is included in the top fluid, the flowing white blood cells (average density $\rho = 1.065$ g/mL) quickly sink to the interface between the 1.070 and 1.085 g/mL fluids where they are neutrally buoyant, and the flowing red blood cells (average density $\rho = 1.10$ g/mL) sink to the interface between the 1.085 and 1.110 g/mL fluids. When the channel splits, the white blood cells flow out of the top outlet and the red blood cells flow out of the bottom outlet.

8.3 Principle of density sorting

In previous work, we showed that when two fluids of different densities flow together horizontally in a microfluidic chip, the fluids quickly reorient themselves relative to gravity (locating the more-dense fluid on the bottom and the less-dense fluid on the top) and form two stable flowing fluid layers of different densities [48]. In this work we show that any number of different-density fluids can be combined in this manner to create a continuously-flowing micron-scale on-chip density gradient capable of sorting cells by their densities. For example, in Figure 8.1, three streams of fluid with three different densities merge together into a single horizontal microfluidic channel. The most-dense fluid (1.110 g/mL) flows along the bottom of the channel; the middle-density fluid (1.085 g/mL) flows along the middle of the channel, and the least-dense fluid (1.070 g/mL) flows along the top of the channel. If one fluid also contains a mixture of cells, then the cells will not only travel horizontally through the channel with the fluid flow but also be move vertically to their isopycnic points due to buoyant forces. For example, if blood cells are added to the least-dense fluid, white blood cells with a density of 1.065 g/mL sink until they reach the interface between the 1.070 and 1.085 g/mL fluids, and red blood cells with a density of 1.10 g/mL sink until the reach the interface between the 1.085 and 1.110 g/mL fluids. When the channel then splits into two outlet channels, the different cell types are sorted to different destinations based on the cells' densities.

To show why our chip is capable of sorting cells by their densities alone (and is not influenced by cell size), we calculated the trajectories followed by cells of different sizes and densities as they flow through the chip. Figure 8.2 shows the trajectories followed by four

different types of objects flowing in two channels containing different fluid density profiles.

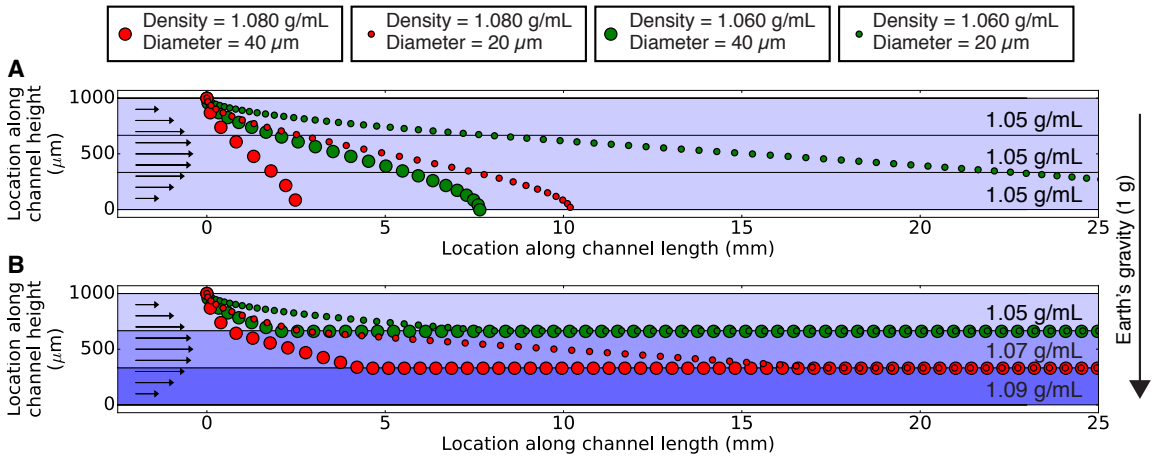

Figure 8.2: Paths followed by four different types of particles in a microchannel containing fluid with a uniform density (**A**; 1.05 g/mL) and in a microchannel containing three zones with different fluid densities (**B**; 1.05, 1.07, and 1.09 g/mL). In both cases, marker color connotes particle density (1.080 g/mL for red; 1.060 g/mL for green), and marker size connotes particle size (40 μm diameter for the larger marker; 20 μm diameter for the smaller marker). The particles all start together at the top of the channel, and the position of each particle is calculated using Equations 1 and 2 at 5 second increments. In a fluid of uniform density (**A**), the particles sink at different speeds but they all end up collecting on the bottom of the channel. However, in a continuously-flowing density gradient (**B**), the green 1.060 g/mL particles sink until they reach the interface between the top two fluid densities, and the red 1.080 g/mL particles sink until they reach the interface between the bottom two fluid densities. The particles then exit the channel in different locations and are thereby sorted according to their density alone (not their size).

The objects are representative of cells with different sizes (10 or 20 μm diameters) and densities (1.060 or 1.080 g/mL). Since the channel contents have a parabolic flow profile (ranging from zero flow at the channel walls to a maximum flow at the center of the channel), the velocity of an object in the x-direction v_x (that is, the object's velocity in the direction of fluid flow) is determined solely by the object's location in the y-direction (its lateral position in the channel):

$$v_x = v_{xmax} \frac{4y\,(h-y)}{h^2} \tag{8.1}$$

where v_{xmax} is the maximum flow velocity in the x direction, h is the height of the channel, and y is the y-coordinate of the location of the object in the channel. Additionally, the velocity of an object in the y-direction v_y (that is, the velocity at which the object floats up or sinks down in the direction of gravity) can be determined by Stokes' Law:

$$\nu_y = \frac{2}{9}\frac{\rho_o - \rho_f}{\mu_f} g r_o^2 \tag{8.2}$$

where ρ_o is the density of the object, ρ_f is the density of the fluid, μ_f is the viscosity of the fluid, g is the gravitational acceleration (-9.8 m/s^2) and r_o the radius of the object. By calculating v_x and v_y over time and plotting y vs. x as shown in Figure 8.2, the paths followed by different cells in the chip can be predicted.

In a microfluidic channel containing fluid with a single uniform density (Fig. 8.2A), cells introduced at the top of the channel follow trajectories that are a function of the cells' sizes *and* densities. For the combination of cell sizes and densities shown, the large and more-dense cells (large red circles) reach the channel floor first. They are then joined by the large and less-dense cells (large green circles), then the small and more-dense cells (small red circles) also reach the channel floor. The small and less-dense cells (small green circles) move the slowest in the y direction and reach the channel floor last, though not within the 25 mm shown. In summary, using fluid of a single uniform density, these four cells cannot be sorted by their densities alone. Instead, the cells eventually accumulate on the channel floor (where, in practical terms, the low flow may cause the cells to be irretrievably stuck in the channel).

However, in a microfluidic channel containing fluid with three different densities (Fig. 8.2B), the four types of cells introduced at the top of the channel reach locations that

are *exclusively* a function of their densities (not their sizes). The large and more-dense cells (large red circles) sink until they reach the interface between the bottom two fluid densities; at this point the cells are neutrally buoyant and no longer move in the y direction but continue flowing in the x direction. The small and more-dense cells (small red circles) take more time to reach the same interface, but once they do, they (and all other cells with the same density) follow the same line as they flow through the channel. Similarly, the large and less-dense cells (large green circles) and small and less-dense cells (small green circles) both converge to the interface between the top two fluid densities. If the channel in Figure 8.2B were to then split in two, the top half would contain only the cells with density = 1.06 (green) and the bottom half would contain only the cells with density = 1.08 g/mL (red). In this manner, by using a microfluidic channel containing fluids of different densities, cells (and other samples) can be continuously sorted by their densities alone.

8.4 Results and Discussion

To validate our method, we used a 3D-printed microfluidic chip to sort microbeads with different densities. The experimental setup and results are summarized in Figure 8.3A. A mixture of polyethylene beads (40 μm diameter; density = 1.025 g/mL) and polystyrene beads (6 μm diameter; density = 1.050 g/mL) was prepared in a physiological buffer (density 1.00 g/mL) and pumped into the top inlet of the chip. The middle inlet received buffer with a density of 1.03 g/mL, and the bottom inlet received buffer with a density of 1.06 g/mL. Small amounts of Percoll (an inert and nontoxic colloidal silica solution) were added to increase the densities of these buffers without significantly affecting their other properties. The fluid

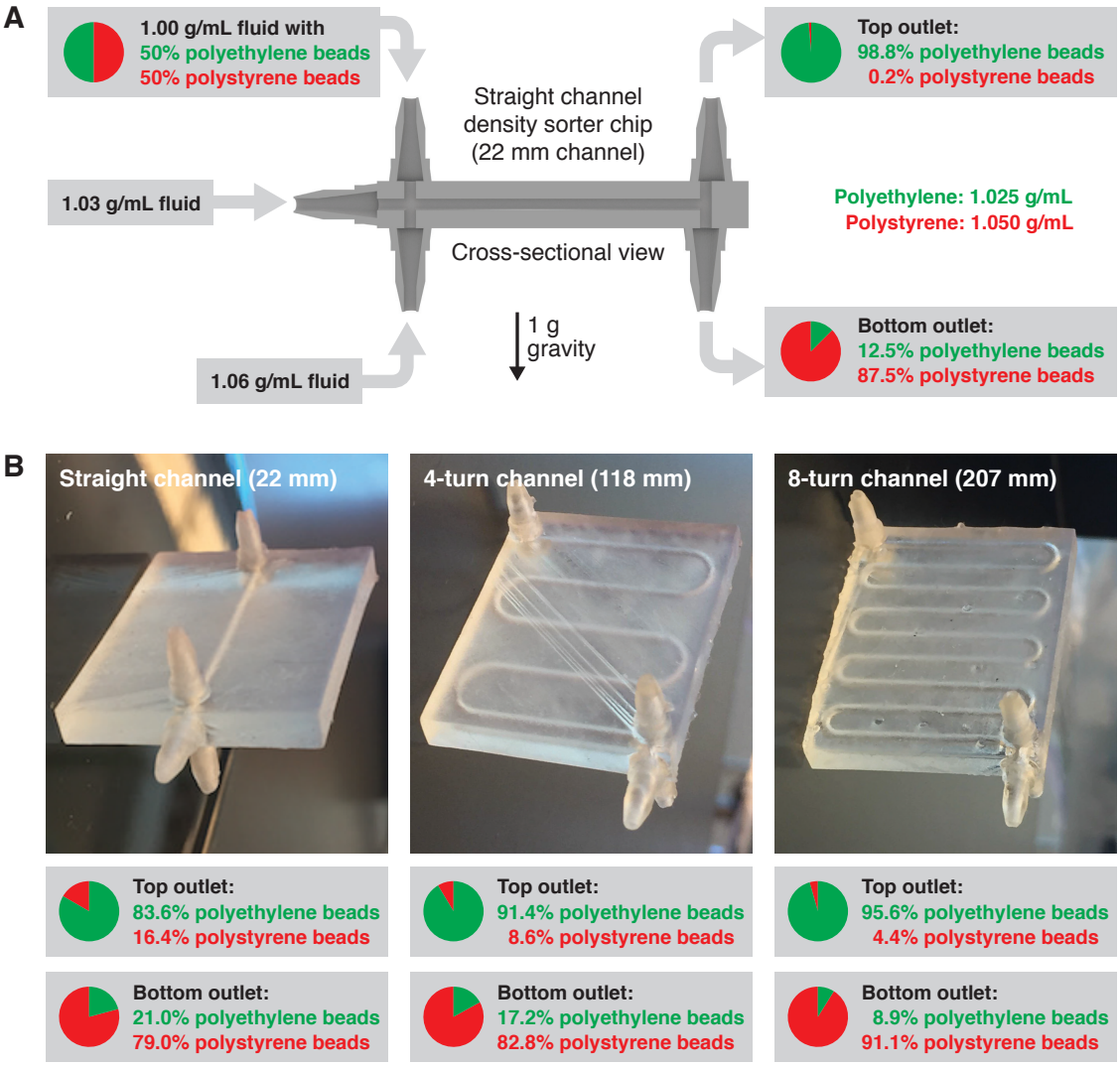

Figure 8.3: (**A**) Sorting microbeads by their density. The inlets of the density sorter chip received fluid of three different densities (1.00 g/mL in the top inlet, 1.03 g/mL in the middle inlet, and 1.06 g/mL in the bottom inlet). The top inlet fluid also contained a 50:50 mixture of polyethylene beads (density 1.025 g/mL) and polystyrene beads (density 1.050 g/mL). The beads collected at the top outlet were 98.8% polyethylene, and the beads collected at the bottom outlet were 87.5% polystyrene. (**B**) To explore the effect of channel length on separation efficiency, the experiment in (A) was repeated but with three different channel lengths (22, 118, and 207 mm) and uniform fluid densities in all three inlets (1.035 g/mL). The results confirm that additional channel length provides more time for density-based separation and improves separation efficiency, with the fraction of polyethylene beads leaving the top outlet increasing from 83.6% to 95.5% and the fraction of polystyrene beads leaving the bottom outlet increasing from 79.0% to 91.1%.

densities were chosen to sort the less-dense polyethylene beads to the interface between the top two fluid densities and sort the more-dense polystyrene beads to the interface between the bottom two fluid densities. Fluid from each outlet was collected and analyzed using a hemocytometer. Of the beads collected from the top outlet, 98.8% were polyethylene and only 0.2% were polystyrene. Conversely, of the beads collected from the bottom outlet, only 12.5% were polyethylene and 87.5% were polystyrene. This demonstrates that the chip can successfully sort beads with only a small (2%) difference in bead density with separation efficiencies approaching 99%.

In principle, giving a bead or other object more time to sink or float to its isopycnic point should improve the separation efficiency of our technique. One way to accomplish this would be to decrease the flow rate through the chip, but this would have the disadvantage of decreasing the throughput of our technique. A better way to accomplish this would be to lengthen the channel containing the flowing density gradient, so the cells spend more time in the gradient before the channel splits. To test whether a longer channel would actually improve our separation efficiency, we fabricated additional chips with serpentine geometries shown in Figure 8.3B. While our original straight-channel chip has a 22 mm long channel containing the flowing density gradient, the four-turn chip has a 118 mm long channel and the eight-turn chip has a 207 mm long channel. To focus exclusively on the effect of channel length, we pumped fluid of a uniform density (1.035 g/mL) into all three inlets, with the top inlet also containing a 50:50 mixture of the same polyethylene and polystyrene beads used above. As expected, additional channel length does improve separation efficiency: lengthening the channel from 22 to 207 mm increased the fraction of polyethylene beads

leaving the top outlet from 83.6% to 95.5% and increased the fraction of polystyrene beads leaving the bottom outlet from 79.0% to 91.1%. Comparing Figure 3A and 3B, we see that the channel containing fluids of three *different* densities (Fig. 23A) outperforms the same-length channel containing a *single* fluid density (Fig. 3B, straight channel), especially for the top outlet (which improves from 83.6% purity to 98.8% purity with the use of three fluid densities). Indeed, the short chip with three fluid densities even outperforms the 8-turn 207 mm long chip with one fluid density in Figure 3B for the purity of the top outlet. These results confirm the value of using multiple fluid densities in density-based cell sorting.

To demonstrate sorting cells by type using their different densities, we used the same 3D-printed microfluidic chip from Figure 3A to sort blood into two fractions: one containing white blood cells (leukocytes), and another containing the other cells (red blood cells and platelets). As shown in Figure 4, buffers with three different densities were pumped into the three inlets of the chip (1.070 g/mL in the top inlet, 1.085 g/mL in the middle inlet, and 1.110 g/mL in the bottom inlet). These fluid densities were chosen to sort the white blood cells (density $1.06 - 1.08$ g/mL) to the interface between the top two fluid densities, and sort the red blood cells ($1.09 - 1.10$ g/mL) to the interface between the bottom two fluid densities. The top buffer also included a 1-in-500 dilution of mouse blood. Cells from each outlet were collected, stained with DAPI (4′,6-diamidino-2-phenylindole; a fluorescent stain that binds to the DNA that is present in white blood cells but absent from red blood cells), and analyzed using fluorescence-activated cell sorter (FACS). Even though white blood cells are relatively rare in mouse blood (only 0.1% of cells [49]), 93.2% of the cells from the top outlet were white blood cells, a nearly 1000× enrichment. The bottom outlet

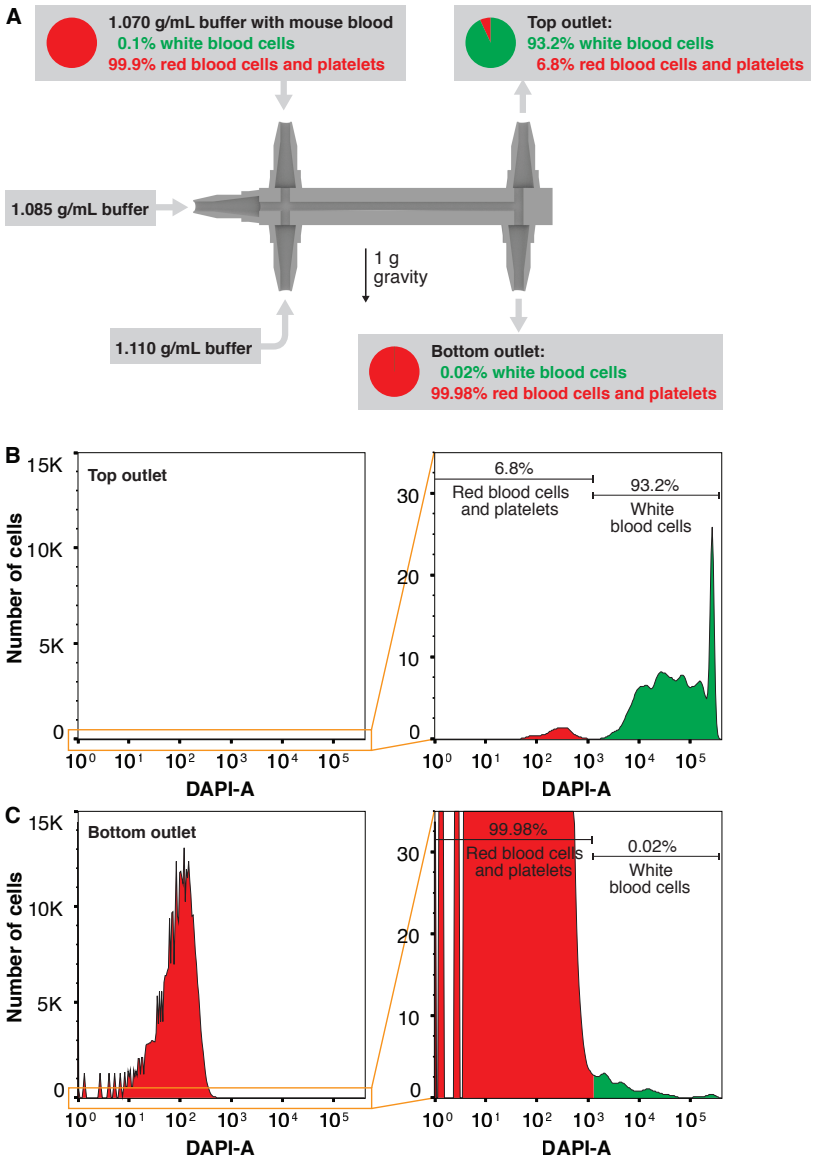

Figure 8.4: Sorting white blood cells from red blood cells and platelets. (**A**) Mouse blood (which normally contains 0.1% white blood cells) was diluted in a 1.070 g/mL buffer and pumped into the top inlet; the middle inlet received 1.085 g/mL buffer and the bottom inlet received 1.110 g/mL buffer. Cells collected at the outlets were then stained using DAPI to distinguish white blood cells from other cells. Flow cytometry analysis of the stained cells indicates 93.2% of the cells exiting the top outlet are white blood cells (**B**); a nearly 1000× enrichment), and 99.98% of the cells exiting the bottom outlet are red blood cells and platelets (**C**).

Table 8.1: Counts of DAPI+ cells (white blood cells) and DAPI− cells (red blood cells and platelets) from three replicates of the blood sorting experiment in Figure 8.4.

	Top outlet		Bottom outlet	
Replicate	DAPI+	DAPI−	DAPI+	DAPI−
1	5764	42	193	7×10^6
2	5599	145	238	6×10^6
3	5280	222	107	6×10^6

contained only 0.02% white blood cells, or about a fifth of the white blood cells present in whole blood. This experiment was performed in triplicate with similar results each time (cell counts shown in Table 1).

The density-based cell sorter presented here offers several advantages over existing techniques like density gradient centrifugation. First, by using a miniaturized density gradient, our chip does not need hundreds or thousands of g's of acceleration to separate cells by their density. Instead, Earth's 1 g is adequate to separate samples with small (2%) differences in density in just a few seconds. Consequently, our technique eliminates the threat of g-force-induced damage to cells and also significantly reduces the cost of our technique and the amount of instrumentation required to perform it. Additionally, our chip uses simple laminar flow to automatically form the desired density gradient on-chip, a significant improvement over centrifugation techniques that require careful manual construction of the gradient. And by using chips with additional inlets supplied with fluids of different densities, continuously-flowing density gradients can be created with any desired density range and resolution. As a continuous-flow technique, our cell sorter eliminates virtually all of the manual labor associated with transferring samples into and collecting fractions out of density gradients.

Finally, since our density sorter chips were fabricated using 3D printing, anyone with access to a printer is welcome to download our design files (Supplementary Information) and use our chips in their own research.

The purity of the cells sorted by our chip (like the 93.2% pure white blood cells isolated from whole blood in Figure 4) is already high enough for many analyses. For applications requiring even higher purity, several density sorter chips could be connected or 3D printed in series, with the desired output from one chip undergoing additional purification in subsequent chips. And for higher throughput (to isolate extremely rare cells of interest like circulating tumor cells), a chip containing hundreds of parallel density sorter chips could be easily fabricated using 3D printing. In this manner, our cell sorter chip is uniquely customizable for applications requiring high purity, high throughput, or both.

8.5 Materials and Methods

Chip design and fabrication. Density sorter chips like the ones shown in Figure 3 were designed using SolidWorks (Dassault Systèmes, Vélizy-Villacoublay, France), exported as an STL file (available for download as Supplementary Information), and printed using a stereolithography-based 3D printer (Form 1+, Formlabs, Cambridge, MA). The chips contain microfluidic channels with 1 mm diameters and varying lengths (a straight 25 mm long channel was used in the experiments in Figures 3A and 4, and 118 and 207 mm long channels were additionally used in the experiments in Figure 3B.

Sorting beads by their density. For the experiment in Figure 3A, polyethylene microbeads (40 μm diameter, 1.025 g/mL density) and polystyrene microbeads (6 μm diameter, 1.05 g/mL density) were obtained from Cospheric (Santa Barbara, CA). The beads were suspended in a buffer containing 1$\times$ phosphate buffered saline (PBS) and 0.05% Tween-20; final solution density 1.00 g/mL. To create the different-density fluids for the middle and bottom inlets, Percoll (GE Life Sciences, Piscataway, NJ) was added to the buffers. Percoll (a non-toxic aqueous solution of $15 - 30$ nm colloidal silica coated with polyvinylpyrrolidone) has a relatively high density (1.13 g/mL) and can be used to adjust the density of a solution without significantly affecting the solution's ionic strength or other properties. In Figure 3A, 5 mL of Percoll were combined with 5.8 mL of 1$\times$ PBS (to create the 1.03 g/mL fluid for the middle inlet) or 16.6 mL of 1$\times$ PBS (to create the 1.06 g/mL fluid for the bottom inlet). All three fluids were loaded into syringe pumps that were connected to the inlets of the 3D-printed chip using Tygon tubbing (Cole-Parmer, Vernon Hills, IL). The buffer containing the beads was injected into the top inlet using a flow rate of 5 μL/min, and the other two fluids were injected into the middle and bottom inlets using a flow rate of 10 μL/min for each. Finally, for the experiments in Figure 3B, all 3 inlets received a 1$\times$ PBS/Percoll solution with a density of 1.035 g/mL.

Sorting blood cells by their density. Blood was drawn from the heart of a healthy mouse according to UC Riverside Institutional Animal Care and Use Committee protocol number A-20140010 into a tube containing the anticoagulant ethylenediaminetetraacetic acid (EDTA). 1μL of blood was suspended in 500μL of 1x PBS buffer containing 4.28 mL of Percoll; final solution density 1.070 g/mL. PBS and Percoll solutions with the densities of

1.085 g/mL and 1.110 g/mL were also prepared in order to generate stacked of three fluid densities. These fluids were pumped into the density sorter chip using the same setup and flow rates as used for the bead experiments.

Chapter 9

Fabrication of the microfluidic "density sorter chip" in glass

In previous chapters, we used a 3D printer to fabricate our "density sorter chip" in order to sort cells. For sorting applications that might require a smaller (truly micron-scale) channel, we also fabricated and tested a density sorter chip using conventional techniques (photolithographic microfabrication of glass) and used the chip to successfully separate polymer microbeads based on their different polymer compositions.

Glass is a popular substrate for microfluidic chips. The most common glass substrate used in the production of microfluidic chips is borosilicate glass because of its optical characteristics (transparent from approximately 350 nm through 700 nm) and its physical properties (annealing temperature of 640°C; resistant to most chemicals). Fabrication of microfluidic chips using borosilicate glass produced by the float method (borofloat glass) involves photolithographic patterning of the channel features onto the photoresist coating

the glass, wet chemical etching of the channel features into the glass, and bonding of the glass to a second glass wafer to complete the channels (Figure 9.1). Each of these steps is explained briefly in the following sections.

Photolithography. The intended channel design is drawn in Adobe Illustrator and printed onto a transparent film using a high resolution printer. The glass used to produce microfluidic chips are intended for the production of photomasks, and are known as photomask blanks. Borofloat photomask blanks are acquired from Telic Company (Santa Monica, CA) with a 530 nm layer of AZ1500 positive photoresist on a thin layer of chrome.

UV Exposure. The UV exposure unit currently used in the lab (IntelliRay 400, Uvitron International, Inc., West Springfield, MA) is intended for contact exposure, meaning a Borofloat photomask blank coated with chrome and positive photoresist was covered by the high resolution photomask containing the desired channel geometry. The photomasks blank presently used in the lab are fabricated such that the chrome surface (brownish-gold in color) should be in contact with the photomask. To secure the photomask to the photomask blank, a piece of plain glass is placed on top of the backside of photomask. The only precaution in the UV exposure step is to ensure that the mask is centered on the blank. Centering the mask prevents overhanging reservoirs in the finished microfluidic chip. The photomask/photomask blank assembly is placed under the UV exposure unit, which has been turned on for at least 5 min to warm up the lamp, and the chip is exposed for a minimum of 5 s at $100 - 120$ mW/cm^2 (Figure 9.1).

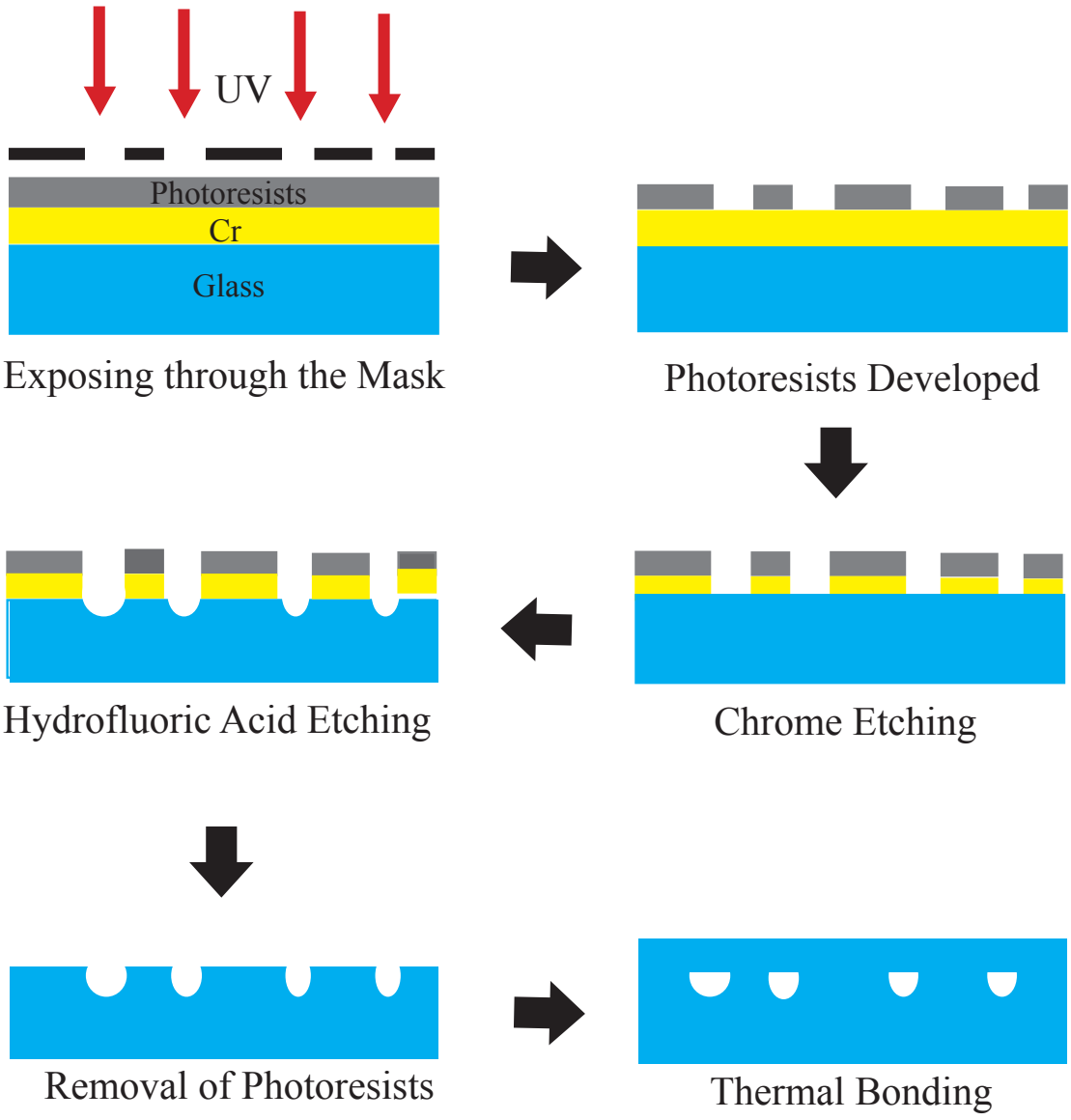

Figure 9.1: Microfabrication process for the glass microfluidic cell separator chip.

Development and Chrome Etching. The exposed photoresist was removed by 0.5% NaOH solution developer and the solution is swirled over the top for couple of minutes and then rinsed with deionized water. The photomask blank is then placed in 25 mL CEP-200 chrome etchant in order to remove exposed chrome. The solution is swirled over the top of the chip until no exposed chrome remains (typically 1-2 min) and then is rinsed with H_2O and dried.

Wet Etching of Glass. The next step in the fabrication procedure is to etch the photomask blank. The photomask blank is then placed in 25 mL of 49% HF solution and the solution is swirled over the top of the photomask blank The etching time is typically around 7 μm/min. The developed photomask blank is rinsed with water, then placed in acetone to remove all remaining photoresist, and then placed in the chrome etching solution to remove all remaining chrome. Now transparent and containing the desired pattern of etched channels, the glass plate is rinsed extensively with deionized water, dried, and brought outside the cleanroom to drill fluidic access holes.

Drilling of Fluidic Access Holes. Before drilling the etched glass is temporarily bonded to a backing piece of glass using pine resin on hot plate. The purpose the pine resin is to hold the etched glass secure during drilling. Using a manual drill (DREMEL 4000), fluidic access holes at the end of each channel are drilled. It is best to drill with the etched channels toward the drill bit as the glass will "pop" out the backside when drilling. After drilling, the etched chip is aggressively rinsed with acetone and water to remove all glass fragments and pine resin.

Figure 9.2: Completed glass microfluidic cell sorter chip.

Bonding Chips. For bonding the glass device we are using a nitrogen-purged muffle furnace (Thermolyne). The assembled chip is placed inside the furnace between two pieces of thick graphite plates. A 500 g stainless steel weight is placed on top of the graphite plates and the temperature is ramped at 10°C/min to 668°C, held for 6-8 hours, and ramped down to room temperature at 10°C/min. Graphite's high melting point, chemical inertness, and lubricity make it a good surface for contacting glass wafers during bonding, but its flammability at high temperatures necessitates the use of nitrogen purge gas during bonding. With this method, high-strength glass-glass bonds can be achieved in a relatively short time without having to use a furnace with complex temperature regulation. In addition, a high degree of optical clarity can be achieved in bonded devices, and no leakage was observed when pumping liquids at high velocities through the microchannels. After bonding, a microscope is used to examine all channels in the chip and then microfluidic reservoirs are applied using epoxy as shown in Figure 9.2.

9.1 Experimental design

The microfluidic "density sorter chip" chip has the capability of extracting specific cells or particles from a sample based solely on the density of the cell or particle. In this chip, two streams of fluid merge together into a single horizontal microfluidic channel. If the chip is oriented on its edge (note direction of gravity in Figure 9.3A) and the lower fluid (red) is more dense than the upper fluid (blue), then a flowing "density bilayer" is formed in the horizontal channel. This density bilayer is stable over a wide range of flow rates and fluid densities because of the combined effects of laminar flow (the absence of turbulent flow in microfluidics) and fluid buoyancy (the more-dense fluid tends to remain on the bottom half of the channel, and the less-dense fluid tends to remain on the top half).

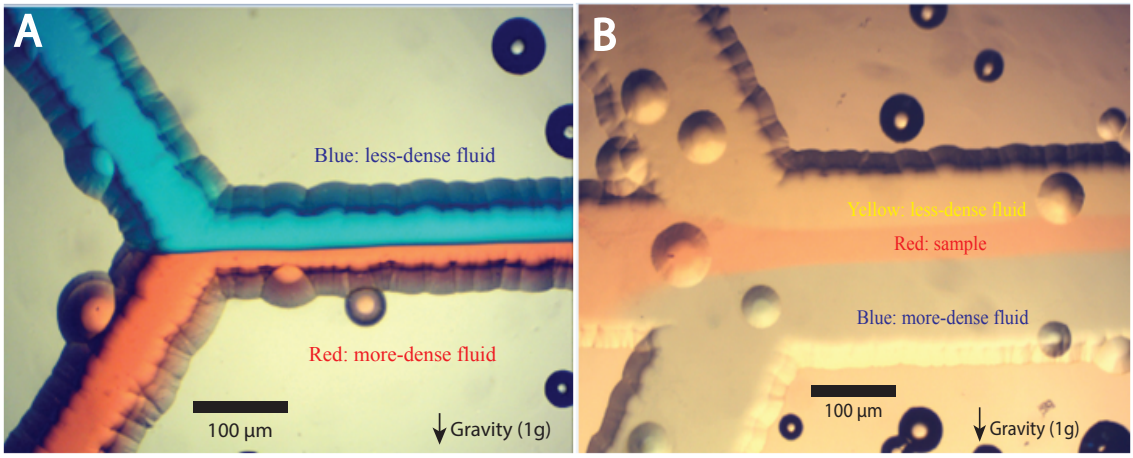

Figure 9.3: Fluids of different densities flowing in a glass density sorter chip. **(A)** Two inlets device with two different fluid densities. **(B)** Three inlets device with with two different fluid densities and sample flowing from middle inlet.

Figure 9.3B shows our fabricated prototype cell density sorter chips in glass. We connected the chip to syringe pumps, and pumped fluids of two different densities through

the chips to confirm that the density bilayer forms as predicted and is stable under various flow conditions Figure 9.3B). A sample of cells (for example, whole blood) can be pumped into the chip from a third input located between the other two. By controlling the relative flow rates of the fluid containing the cells and the density bilayer forming fluids, the cell-containing fluid can be "pinched" very thin, so thin that the cells flow in a line along the interface between the two fluids in the density bilayer.

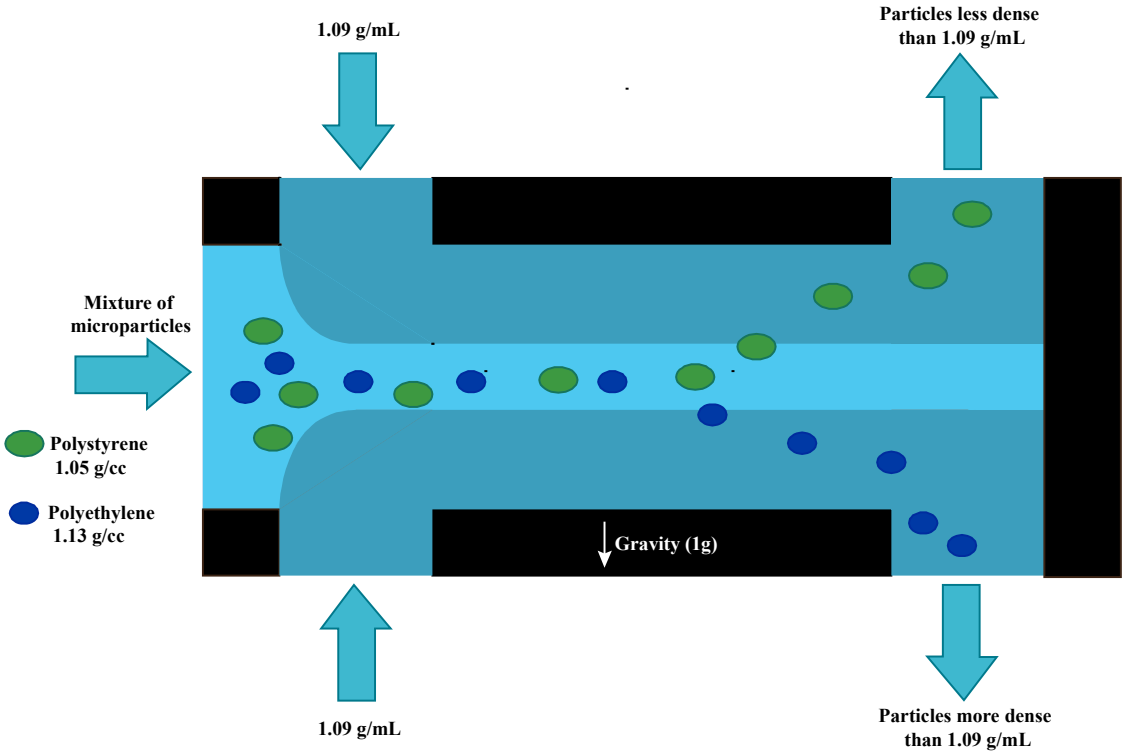

Figure 9.4: Prototype "density sorter chip" for microbead sorting. The microbeads are introduced into the microchannel through the middle inlet with the volume flow rate Q_{sample} =1.0 μL/min and focused by the sheath flow rate Q_{sheath} = 3 μL/min from the other two inlets. The beads are collected in the outlets.

9.2 Preliminary Results

A prototype glass density sorter chip was fabricated with 3 inlets, 2 outlets, and a channel length of 60mm. Particles were injected from the middle inlet into the channel with the sample flow rate (Q_{sample}) and focused by the sheath flow (Q_{sheath}).

9.3 Microsphere Sorting

To demonstrate sorting capability of the glass chip, microspheres with different densities were used. Polyethylene beads (18 μm, 1.13 g/cc) and polystyrene beads (6 μm, 1.05 g/cc) obtained from CoSpheric (Santa Barbara, CA) were prepared by diluting the solid microspheres in Tween 20 and 1% phosphate buffered saline (PBS); pH = 7.4 and solution density = 1.00 g/mL. Tween 20 was added in order to prevent any particle-particle adhesion. The particles were injected from the middle inlet into the channel and focused by two sheath flow densities of 1.09 g/mL. Microspheres were collected in the two outlets at the end.

An illustration of the density sorter chip is shown in Figure 9.5. The chip is oriented on its edge (in the direction of gravity) and the sample is being infused from the top syringe pump with the rate of 1 μL/min (Figure 9.5). The left syringe pump controls the inflow with the Q_{sheath} of 3 μL/min. The right pump collects the microspheres in each syringe at the flow rates of 3.5 μL/min fluid. When beads flow into the density bilayer, polyethylene beads with density of 1.13 g/mL sink in the sheath fluid and polystyrene beads with density of 1.05 g/mL will float in the sheath fluid. At the end of the channel the beads

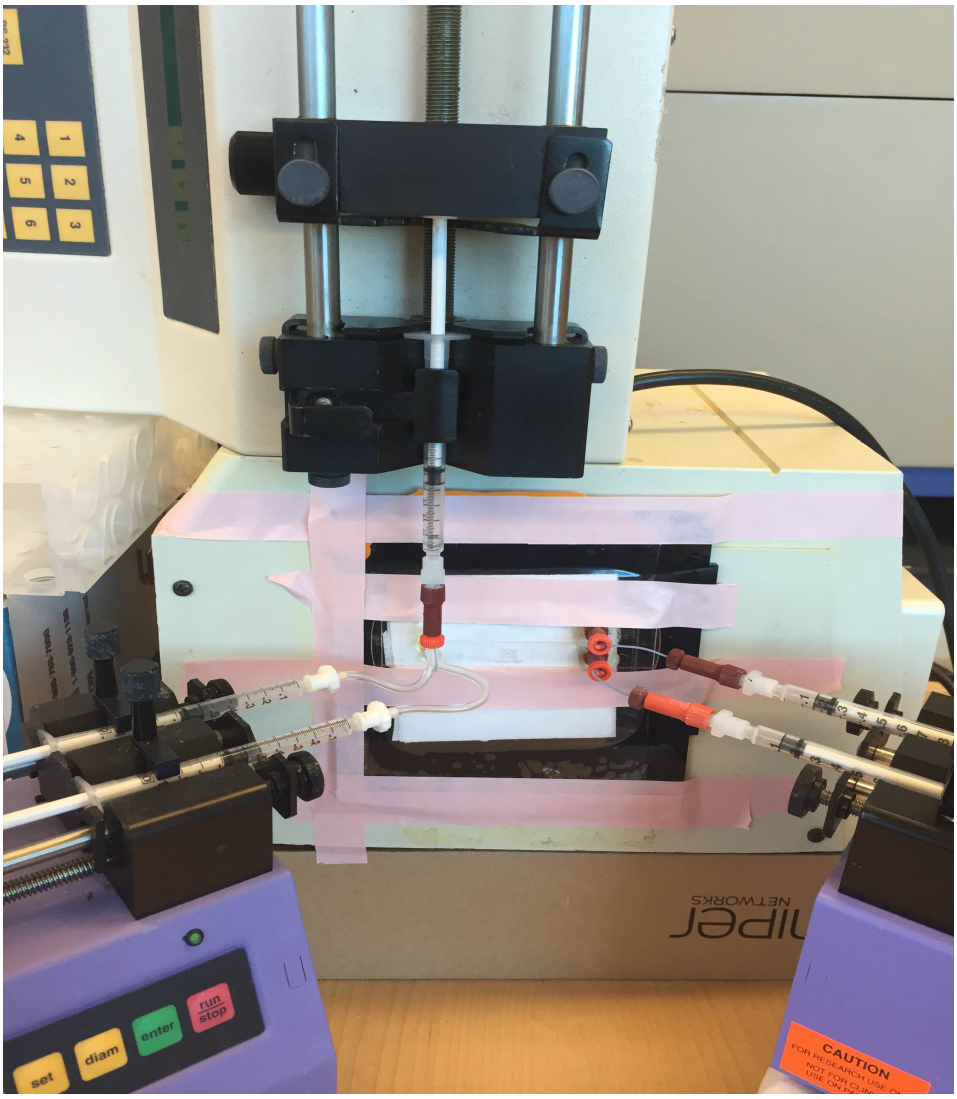

Figure 9.5: Operation of the "density sorter chip" sorting two microspheres with different densities.

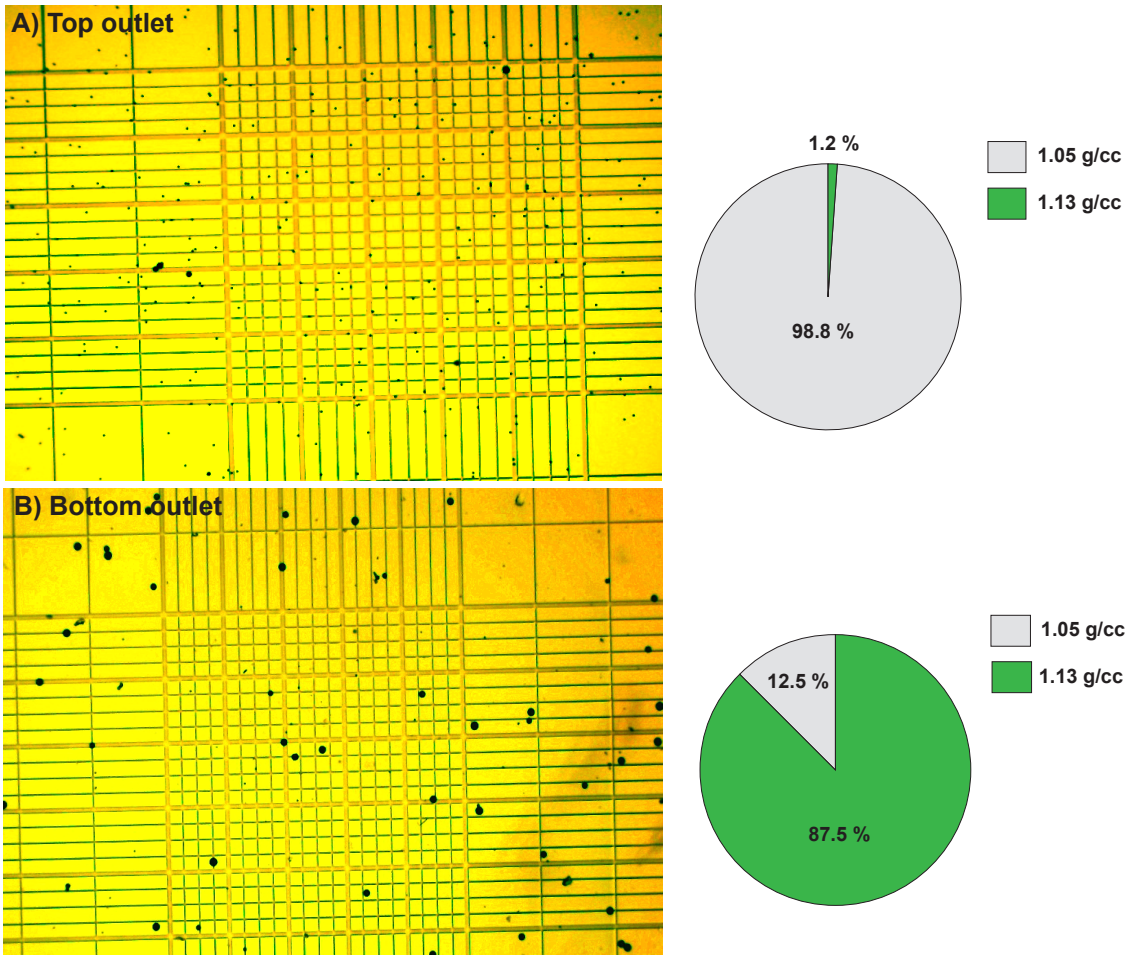

Figure 9.6: Hemocytometer images of the microspheres collected from the glass density sorter chip. **(A)** The top outlet contained 98.8% polystyrene beads with a density of 1.05 g/mL. **(B)** The bottom outlet contained 87.5% polyethylene beads with a density of 1.13 g/mL.

were collected in the outlets. Images from the hemocytometer chip (Figure 9.6) confirm that the more-dense polyethylene beads collected in the bottom outlet and the less-dense polystyrene beads collected in the top outlet.

Chapter 10

Conclusions and Future work

Biological and clinical samples are often heterogeneous populations of many different types of cells. Blood, for example, is a complex mixture of different cell types, only one of which may be needed for a given application. As a result, the ability to separate and sort cells by their type is fundamentally important in modern biological research and medical diagnostics. Label-free techniques for cell separation and sorting can potentially be applied to a much wider range of cell types and usually don't only rely on differences in the fundamental physical properties of the cells to be sorted. Of all the physical properties of cells that could be used to distinguish and separate cells of interest, cell density—the mass-to-volume ratio of the cell—is the most powerful.

Here, we demonstrated a technique for on-chip fluid control that requires no off-chip hardware. We accomplish this by using inert compounds to adjust the densities of fluids in the chip. We found that when fluids of different densities flow together under laminar flow, the interface between the fluids quickly reorients to be orthogonal to Earth's

gravitational force. If the channel containing the fluids then splits into two channels, the amount of each fluid flowing into each channel is precisely determined by the angle of the channels relative to gravity. Thus, any fluid can be routed in any direction and mixed in any desired ratio on-chip simply by holding the chip at a certain angle. This approach allows for sophisticated control of on-chip fluids with no off-chip control hardware, significantly reducing the cost of microfluidic instruments in point-of-care or resource-limited settings.

We also used multi-density fluid flows in our "density sorter chip," which is capable of separating rare cells (white blood cells) from a complex mixture of cells (blood) without the need for density gradient centrifugation. Our method can be used to precisely sort the rare cell of interest based on density and can eliminate a substantial portion of the cost, size, and power-consumption of a microfluidic assay or instrument.

This technique can easily be applied to separate CTCs from blood based on the fact that CTCs typically have a different density than other blood cells. Different types of cancers produce CTCs with different characteristics, and currently no single technique can be used to isolate and detect all types of CTCs. Rather, each technique needs to be optimized for a particular cancer type. However our "density sorter chip" could be used to separate and sort CTCs based on their densities, over a wider range of cancer types.

In this section, we describe how we can leverage microfluidic mass sensor called a Suspended Microchannel Resonator (SMR) to measure the buoyant mass of each CTC for our "density sorter chip" technique .

10.1 Measure the density of cells in whole blood spiked with simulated CTCs from prostate, breast, and colorectal cancers

To separate CTCs and blood cells based on their density, it is first necessary to know precisely the density of CTCs and blood cells to confirm that they are in fact different. The density difference between most CTCs and blood cells is the basis for existing density gradient centrifugation-based tools for CTC isolation, so we fully expect to observe a density difference between CTCs and blood cells. However, the densities of different CTCs have not yet be measured accurately.

Our existing single-cell density measurement system can be used to precisely measure the density of simulated CTCs and various other healthy cell types present in blood (erythrocytes, thrombocytes, lymphocytes, and non-cancerous epithelial cells). We will use a microfluidic mass sensor called a Suspended Microchannel Resonator (SMR) to measure the buoyant mass of each cell in two fluids of different density. [50] From these two buoyant mass measurements, the mass, volume, and density of each cell can be calculated. [21]

By using commercial kits to extract other cell types of interest from whole blood, and then using our SMR technique to measure the density of these cell types, we will obtain what may be the most precise measurements of blood cell densities to date.

This technique can also be used to measure the single-cell densities of three cultered cancer cell lines that are representative of actual CTCs: PC3 (prostate cancer), SKBR3 (breast cancer), and HT-29 (colorectal cancer). Based on our measured values of cell density

for CTCs and healthy blood cells, we will define the range of densities in which we expect to find CTCs.

10.2 Experimental Design

In previous work we utilized the SMR mass sensor to measure the mass, volume and density of single cells. The SMR is capable of weighing micron-scale objects with femtogram resolution. The sensor consists of a microfabricated silicon cantilever in which a microfluidic channel is embedded. The cantilever vibrates at a resonance frequency that is inversely proportional to its mass. When a micron-scale object like a cell passes through the embedded microfluidic channel, the resonance frequency of the cantilever changes by an amount proportional to the buoyant mass of the object. By measuring this transient change in resonance frequency as an object passes through the cantilever, the buoyant mass of the object is determined.

Whole blood will be obtained from a healthy mouse under a research protocol and stored at 4°C until analysis. 5 μL of whole blood will be diluted into 10mL of 1X PBS. To make the more-dense buffer, 100μL of 10X PBS will be combined with 900μL of high-density Percoll. The diluted blood samples are maintained at 25°C during analysis.

10.3 Density measurements of red blood cells, white blood cells and CTCs using the SMR

To measure single red/white blood cell density with the SMR, the device is first loaded with two different fluids: one containing the cells of interest in PBS (red in Figure

10.1), and another with a greater density, in this case a Percoll solution (blue in Figure 10.1). The density of the red fluid is determined from the resonance frequency of the cantilever while filled with red fluid (Figure 10.1, step 1). A cell's buoyant mass in the red fluid is then recorded from the height of the peak in the resonance frequency while the cell passes through the cantilever (Figure 10.1, step 2). The cell then enters the blue fluid, where the faster flow rate quickly dilutes and replaces the red fluid surrounding the cell. Fluid exchange surrounding a single cell happens in $\sim$ 1 s under laminar flow conditions. The direction of flow is then reversed, blue fluid fills the cantilever (Figure 10.1, step 3), and the cell passes through the cantilever a second time to measure its buoyant mass in the blue fluid (Figure 10.1, step 4).

From these two measurements of buoyant mass, the absolute mass, volume, and density of the cell can be calculated. This process takes approximately 5 s per cell, and the system can measure approximately 500 cells per hour.

10.4 Fabricate and test a novel microfluidic device for continuous-flow separation of CTCs from blood based solely on their density

Here, we will use the cell density measurements from previous step to optimize the microfluidic chip developed in previous section for separation and capture of CTCs cancer-cell-spike from whole blood. This CTC-chip is unique in that it sorts rare cells directly from whole blood in a single step in milliliter-scale volumes. By knowing the actual cell

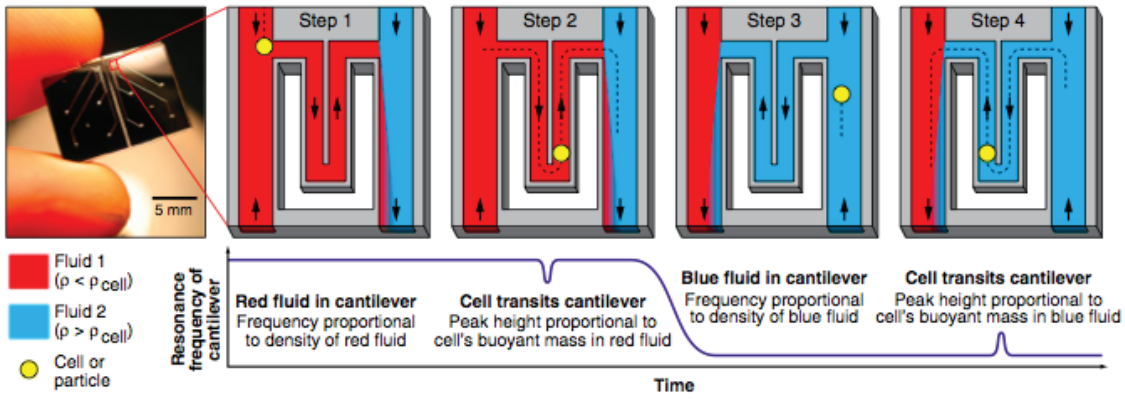

Figure 10.1: Using the SMR (left) to measure the mass, volume, and density of a cell in two fluids of different densities. Measurement starts with the cantilever filled with any buffer or media less dense than the cell (red, step 1). The density of the red fluid is determined from the baseline resonance frequency of the cantilever. When a cell passes through the cantilever (step 2), the buoyant mass of the cell in the red fluid is calculated from the height of the peak in the resonance frequency. The direction of fluid flow is then reversed, and the resonance frequency of the cantilever drops as the cantilever fills with a fluid more dense than the cell (blue, step 3). The buoyant mass of the cell in the blue fluid is measured as the cell transits the cantilever a second time (step 4). From these four measurements of fluid density and cell buoyant mass, the absolute mass, volume, and density of the cell are calculated.

densities from the previous section we can calculate the fluid densities required for sorting CTCs from whole blood.

A 3D printed "density sorter chip" will be fabricated using the same fabrication method explained in Chapter 4. A sample of whole blood containing CTCs is introduced into the chip from a third input located between the other two (Figure 10.2) using syringe pump. By controlling the relative flow rates of the fluid containing the cells and the density bilayer-forming fluids controlled by syringe pumps, the cell-containing fluid can be "pinched" very thin, so thin that the cells flow in a thin line along the interface between the two fluids in the density bilayer. We will use a combination of Percoll and PBS as a sheath fluid to control the movements of different cells inside the channel. As described previously, the sample inlet will be connected to a syringe pump using PVC tubes, and the other two sheath inlets and outlets also will be connected independently to a syringe pump using the same tubing.

As the cells flow along the interface between the two fluid densities, cells that are more dense than the lower fluid (*e.g.*, red blood cells) leave the interface and sink slightly into the lower fluid. Additionally, cells that are less dense than the upper fluid (CTCs) leave the interface and float slightly into the upper fluid. The only cells left in the interface at the end of the horizontal channel are those whose density is between the densities of the two fluids which are the white blood cells. At its end, the horizontal channel splits into three exit channels that contain cells with densities in the desired range (middle channel), cells with higher densities (upper channel), and cells with lower densities (lower channel) as shown in Figure 10.3.

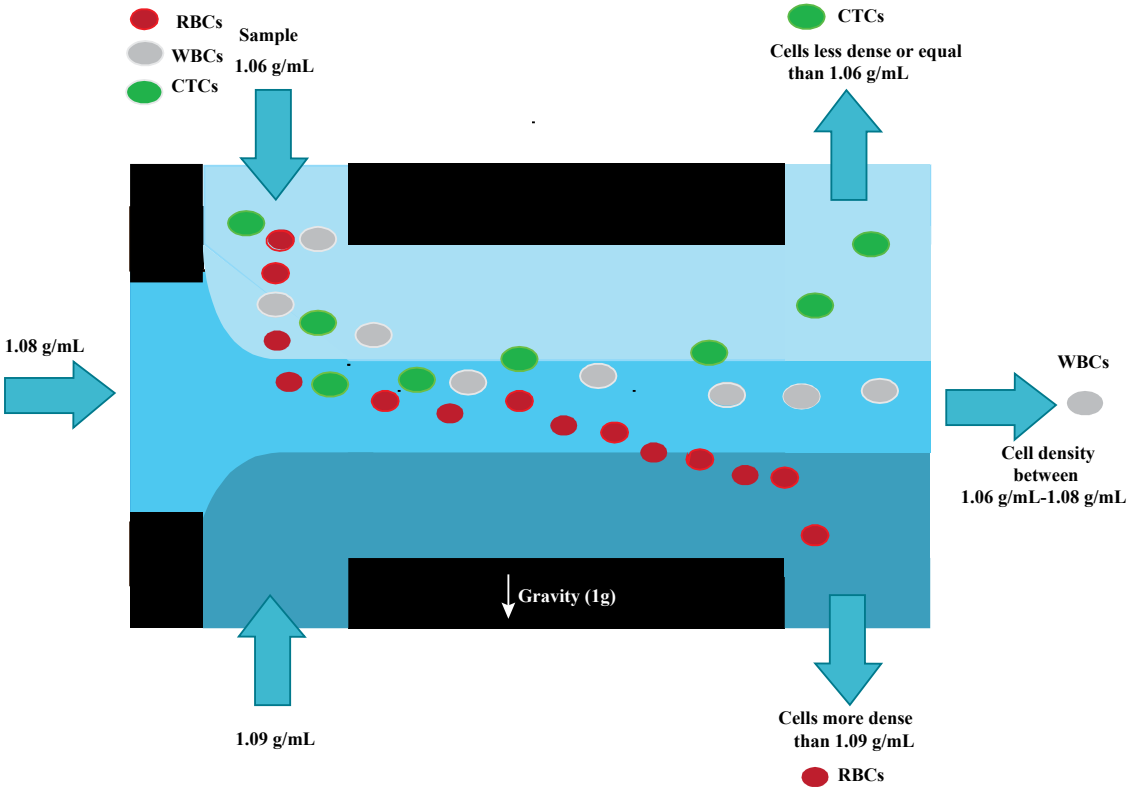

Figure 10.2: Illustration of a 3D microfluidic "density sorter chip" with 3 inlets and 3 outlets sorting CTCs from other cells in whole blood.

Separated CTCs can then be collected for enumeration, additional studies, or even possible transfusion of CTC-free fractions of blood cells back into a patient for therapeutic uses (Figure 10.3). The simplicity of both sample manipulation make this technique straightforwardly applicable in clinical use. The viability of CTCs after collection is an important factor that enables researchers to reveals information about cancer progress and metastasis. This method will allow for the collection of CTCs without sample loss or excessive dilution.

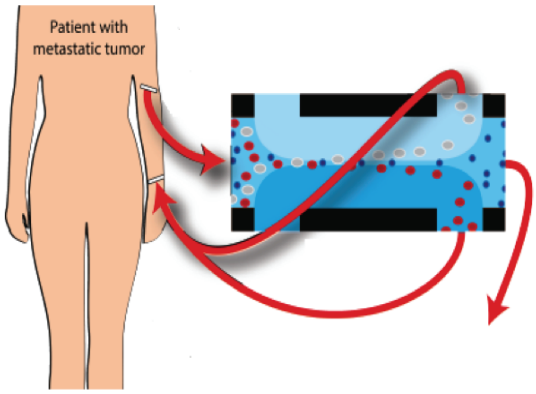

Figure 10.3: A possible therapeutic use for the density sorter chip, removing CTCs from the blood of a patient with metastatic tumor and infusing "clean" blood back into the patient.

We also will be able to modify the design of our "density sorter chip" for better enrichment and purity. 3D-printing will give us the ability to make any arbitrary geometry and leverage the third dimension to make "density sorter cubes." By fabricating long or parallel channels we can increase the throughput and resolution of our CTC sorting.

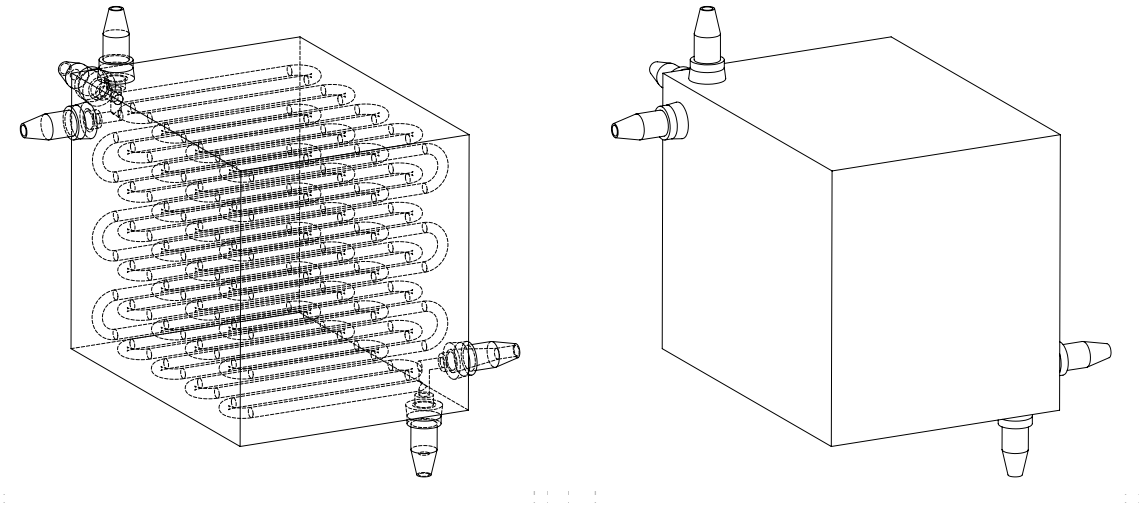

Figure 10.4: Design of a high-throughput "density sorter cube" for isolating CTCs in blood. 3D printers make it possible to consider microfluidic designs that would be impossible to create using traditional fabrication methods.

Bibliography

[1] Shyamala Maheswaran and Daniel A Haber. Circulating tumor cells: a window into cancer biology and metastasis. *Current opinion in genetics & development*, 20(1):96–99, 2010.

[2] Patrizia Paterlini-Brechot and Naoual Linda Benali. Circulating tumor cells (ctc) detection: clinical impact and future directions. *Cancer letters*, 253(2):180–204, 2007.

[3] Edoardo Botteri, Maria Teresa Sandri, Vincenzo Bagnardi, Elisabetta Munzone, Laura Zorzino, Nicole Rotmensz, Chiara Casadio, Maria Cristina Cassatella, Angela Esposito, Giuseppe Curigliano, et al. Modeling the relationship between circulating tumour cells number and prognosis of metastatic breast cancer. *Breast cancer research and treatment*, 122(1):211–217, 2010.

[4] Jean-Yves Pierga, François-Clément Bidard, Claire Mathiot, Etienne Brain, Suzette Delaloge, Sylvie Giachetti, Patricia de Cremoux, Rémy Salmon, Anne Vincent-Salomon, and Michel Marty. Circulating tumor cell detection predicts early metastatic relapse after neoadjuvant chemotherapy in large operable and locally advanced breast cancer in a phase ii randomized trial. *Clinical Cancer Research*, 14(21):7004–7010, 2008.

[5] Yong S Chang, Emmanuelle di Tomaso, Donald M McDonald, Rosemary Jones, Rakesh K Jain, and Lance L Munn. Mosaic blood vessels in tumors: frequency of cancer cells in contact with flowing blood. *Proceedings of the National Academy of Sciences*, 97(26):14608–14613, 2000.

[6] Marija Balic, Nadia Dandachi, Günter Hofmann, Hellmut Samonigg, Hans Loibner, Andreas Obwaller, Alexander van der Kooi, Arjan GJ Tibbe, Gerald V Doyle, Leon WMM Terstappen, et al. Comparison of two methods for enumerating circulating tumor cells in carcinoma patients. *Cytometry Part B: Clinical Cytometry*, 68(1):25–30, 2005.

[7] T Fehm, EF Solomayer, S Meng, T Tucker, N Lane, J Wang, and G Gebauer. Methods for isolating circulating epithelial cells and criteria for their classification as carcinoma cells. *Cytotherapy*, 7(2):171–185, 2005.

[8] R Rosenberg, R Gertler, J Friederichs, K Fuehrer, M Dahm, R Phelps, S Thorban, H Nekarda, and JR Siewert. Comparison of two density gradient centrifugation systems for the enrichment of disseminated tumor cells in blood. *Cytometry*, 49(4):150–158, 2002.

[9] Giovanna Vona, Abdelmajid Sabile, Malek Louha, Veronique Sitruk, Serge Romana, Karin Schütze, Frédérique Capron, Dominique Franco, Mario Pazzagli, Michel Vekemans, et al. Isolation by size of epithelial tumor cells: a new method for the immunomorphological and molecular characterization of circulating tumor cells. *The American journal of pathology*, 156(1):57–63, 2000.

[10] Volkmar Müller, Nicole Stahmann, Sabine Riethdorf, Thomas Rau, Tanja Zabel, Alexander Goetz, Fritz Jänicke, and Klaus Pantel. Circulating tumor cells in breast cancer: correlation to bone marrow micrometastases, heterogeneous response to systemic therapy and low proliferative activity. *Clinical Cancer Research*, 11(10):3678–3685, 2005.

[11] Sabine Riethdorf, Herbert Fritsche, Volkmar Müller, Thomas Rau, Christian Schindlbeck, Brigitte Rack, Wolfgang Janni, Cornelia Coith, Katrin Beck, Fritz Jänicke, et al. Detection of circulating tumor cells in peripheral blood of patients with metastatic breast cancer: a validation study of the cellsearch system. *Clinical Cancer Research*, 13(3):920–928, 2007.

[12] Kazunori Hoshino, Yu-Yen Huang, Nancy Lane, Michael Huebschman, Jonathan W Uhr, Eugene P Frenkel, and Xiaojing Zhang. Microchip-based immunomagnetic detection of circulating tumor cells. *Lab on a Chip*, 11(20):3449–3457, 2011.

[13] W Jeffrey Allard, Jeri Matera, M Craig Miller, Madeline Repollet, Mark C Connelly, Chandra Rao, Arjan GJ Tibbe, Jonathan W Uhr, and Leon WMM Terstappen. Tumor cells circulate in the peripheral blood of all major carcinomas but not in healthy subjects or patients with nonmalignant diseases. *Clinical Cancer Research*, 10(20):6897–6904, 2004.

[14] Anieta M Sieuwerts, Jaco Kraan, Joan Bolt, Petra van der Spoel, Fons Elstrodt, Mieke Schutte, John WM Martens, Jan-Willem Gratama, Stefan Sleijfer, and John A Foekens. Anti-epithelial cell adhesion molecule antibodies and the detection of circulating normal-like breast tumor cells. *Journal of the National Cancer Institute*, 101(1):61–66, 2009.

[15] Sunitha Nagrath, Lecia V Sequist, Shyamala Maheswaran, Daphne W Bell, Daniel Irimia, Lindsey Ulkus, Matthew R Smith, Eunice L Kwak, Subba Digumarthy, Alona Muzikansky, et al. Isolation of rare circulating tumour cells in cancer patients by microchip technology. *Nature*, 450(7173):1235–1239, 2007.

[16] Shannon L Stott, Chia-Hsien Hsu, Dina I Tsukrov, Min Yu, David T Miyamoto, Belinda A Waltman, S Michael Rothenberg, Ajay M Shah, Malgorzata E Smas, George K Korir, et al. Isolation of circulating tumor cells using a microvortex-generating

herringbone-chip. *Proceedings of the National Academy of Sciences*, 107(43):18392–18397, 2010.

[17] Shutao Wang, Kan Liu, Jian Liu, Zeta T-F Yu, Xiaowen Xu, Libo Zhao, Tom Lee, Eun Kyung Lee, Jean Reiss, Yi-Kuen Lee, et al. Highly efficient capture of circulating tumor cells by using nanostructured silicon substrates with integrated chaotic micromixers. *Angewandte Chemie International Edition*, 50(13):3084–3088, 2011.

[18] Frederick F Becker, Xiao-Bo Wang, Ying Huang, Ronald Pethig, Jody Vykoukal, and PR Gascoyne. Separation of human breast cancer cells from blood by differential dielectric affinity. *Proceedings of the National Academy of Sciences*, 92(3):860–864, 1995.

[19] John A Davis, David W Inglis, Keith J Morton, David A Lawrence, Lotien R Huang, Stephen Y Chou, James C Sturm, and Robert H Austin. Deterministic hydrodynamics: taking blood apart. *Proceedings of the National Academy of Sciences*, 103(40):14779–14784, 2006.

[20] Palaniappan Sethu, Aaron Sin, and Mehmet Toner. Microfluidic diffusive filter for apheresis (leukapheresis). *Lab on a Chip*, 6(1):83–89, 2006.

[21] William H Grover, Andrea K Bryan, Monica Diez-Silva, Subra Suresh, John M Higgins, and Scott R Manalis. Measuring single-cell density. *Proceedings of the National Academy of Sciences*, 108(27):10992–10996, 2011.

[22] Ralf Gertler, Robert Rosenberg, Katrin Fuehrer, Michael Dahm, Hjalmar Nekarda, and Joerg Ruediger Siewert. Detection of circulating tumor cells in blood using an optimized density gradient centrifugation. In *Molecular Staging of Cancer*, pages 149–155. Springer, 2003.

[23] Marc A Unger, Hou-Pu Chou, Todd Thorsen, Axel Scherer, and Stephen R Quake. Monolithic microfabricated valves and pumps by multilayer soft lithography. *Science*, 288(5463):113–116, 2000.

[24] William H Grover, Alison M Skelley, Chung N Liu, Eric T Lagally, and Richard A Mathies. Monolithic membrane valves and diaphragm pumps for practical large-scale integration into glass microfluidic devices. *Sensors and Actuators B: Chemical*, 89(3):315–323, 2003.

[25] Joel Voldman. Electrical forces for microscale cell manipulation. *Annu. Rev. Biomed. Eng.*, 8:425–454, 2006.

[26] Frieder Mugele and Jean-Christophe Baret. Electrowetting: from basics to applications. *Journal of Physics: Condensed Matter*, 17(28):R705, 2005.

[27] Christopher G Cooney, Chao-Yi Chen, Michael R Emerling, Ali Nadim, and James D Sterling. Electrowetting droplet microfluidics on a single planar surface. *Microfluidics and Nanofluidics*, 2(5):435–446, 2006.

[28] S Hardt, H Pennemann, and F Schönfeld. Theoretical and experimental characterization of a low-reynolds number split-and-recombine mixer. *Microfluidics and Nanofluidics*, 2(3):237–248, 2006.

[29] Peter E Neerincx, Roel PJ Denteneer, Sven Peelen, and Han EH Meijer. Compact mixing using multiple splitting, stretching, and recombining flows. *Macromolecular Materials and Engineering*, 296(3-4):349–361, 2011.

[30] Brian M Paegel, William H Grover, Alison M Skelley, Richard A Mathies, and Gerald F Joyce. Microfluidic serial dilution circuit. *Analytical chemistry*, 78(21):7522–7527, 2006.

[31] Choong Kim, Kangsun Lee, Jong Hyun Kim, Kyeong Sik Shin, Kyu-Jung Lee, Tae Song Kim, and Ji Yoon Kang. A serial dilution microfluidic device using a ladder network generating logarithmic or linear concentrations. *Lab on a Chip*, 8(3):473–479, 2008.

[32] Johan Pihl, Jon Sinclair, Eskil Sahlin, Mattias Karlsson, Fredrik Petterson, Jessica Olofsson, and Owe Orwar. Microfluidic gradient-generating device for pharmacological profiling. *Analytical Chemistry*, 77(13):3897–3903, 2005.

[33] Shinji Sugiura, Koji Hattori, and Toshiyuki Kanamori. Microfluidic serial dilution cell-based assay for analyzing drug dose response over a wide concentration range. *Analytical chemistry*, 82(19):8278–8282, 2010.

[34] Casey M Karst, Brian D Storey, and John B Geddes. Laminar flow of two miscible fluids in a simple network. *Physics of Fluids (1994-present)*, 25(3):033601, 2013.

[35] AI Boyum. Isolation of mononuclear cells and granulocytes from human peripheral blood. *Scand j clin lab invest*, 21(97):77–89, 1968.

[36] Håkan Pertoft, Kristofer Rubin, Lena Kjellén, Torvard C Laurent, and Berndt Klingeborn. The viability of cells grown or centrifuged in a new density gradient medium, percoll (tm). *Experimental cell research*, 110(2):449–457, 1977.

[37] BH Grynne, JØ Nossen, B Bolstad, and KW Borch. Main results of the first comparative clinical studies on visipaque an overview of 18 clinical studies. *Acta Radiologica*, 36(399 suppl):265–270, 1995.

[38] Yi-Chin Toh, Teck Chuan Lim, Dean Tai, Guangfa Xiao, Danny van Noort, and Hanry Yu. A microfluidic 3d hepatocyte chip for drug toxicity testing. *Lab on a Chip*, 9(14):2026–2035, 2009.

[39] Stefan Miltenyi, Werner Müller, Walter Weichel, and Andreas Radbruch. High gradient magnetic cell separation with macs. *Cytometry*, 11(2):231–238, 1990.

[40] Ashok Kumar and Aditi Bhardwaj. Methods in cell separation for biomedical application: cryogels as a new tool. *Biomedical materials*, 3(3):034008, 2008.

[41] Kushang V Patel, Luigi Ferrucci, William B Ershler, Dan L Longo, and Jack M Guralnik. Red blood cell distribution width and the risk of death in middle-aged and older adults. *Archives of internal medicine*, 169(5):515–523, 2009.

[42] Larry A Allen, G Michael Felker, Mandeep R Mehra, Jun R Chiong, Stephanie H Dunlap, Jalal K Ghali, Daniel J Lenihan, Ron M Oren, Lynne E Wagoner, Todd A Schwartz, et al. Validation and potential mechanisms of red cell distribution width as a prognostic marker in heart failure. *Journal of cardiac failure*, 16(3):230–238, 2010.

[43] Jeffrey R SooHoo and Glenn M Walker. Microfluidic aqueous two phase system for leukocyte concentration from whole blood. *Biomedical microdevices*, 11(2):323–329, 2009.

[44] Elodie Sollier, Hervé Rostaing, Patrick Pouteau, Yves Fouillet, and Jean-Luc Achard. Passive microfluidic devices for plasma extraction from whole human blood. *Sensors and Actuators B: Chemical*, 141(2):617–624, 2009.

[45] Neil R Sims and Michelle F Anderson. Isolation of mitochondria from rat brain using percoll density gradient centrifugation. *Nature protocols*, 3(7):1228–1239, 2008.

[46] Shunichi Fukuda and Geert W Schmid-Schönbein. Centrifugation attenuates the fluid shear response of circulating leukocytes. *Journal of leukocyte biology*, 72(1):133–139, 2002.

[47] A Bøyum. Isolation of lymphocytes, granulocytes and macrophages. *Scandinavian Journal of Immunology*, 5(s5):9–15, 1976.

[48] Nazila Norouzi, Heran C Bhakta, and William H Grover. Orientation-based control of microfluidics. *PloS one*, 11(3):e0149259, 2016.

[49] JA Nemzek, GL Bolgos, BA Williams, and DG Remick. Differences in normal values for murine white blood cell counts and other hematological parameters based on sampling site. *Inflammation research*, 50(10):523–527, 2001.

[50] Michel Godin, Francisco Feijó Delgado, Sungmin Son, William H Grover, Andrea K Bryan, Amit Tzur, Paul Jorgensen, Kris Payer, Alan D Grossman, Marc W Kirschner, et al. Using buoyant mass to measure the growth of single cells. *Nature methods*, 7(5):387–390, 2010.

[51] Javier Atencia and David J Beebe. Steady flow generation in microcirculatory systems. *Lab on a Chip*, 6(4):567–574, 2006.

[52] Himisha Beltran, Adam Jendrisak, Mark Landers, Juan Miguel Mosquera, Myriam Kossai, Jessica Louw, Rachel Krupa, Ryon P Graf, Nicole A Schreiber, David M Nanus, et al. The initial detection and partial characterization of circulating tumor cells in neuroendocrine prostate cancer. *Clinical Cancer Research*, 2015.

[53] Stefan Haeberle, Thilo Brenner, Roland Zengerle, and Jens Ducrée. Centrifugal extraction of plasma from whole blood on a rotating disk. *Lab on a Chip*, 6(6):776–781, 2006.

[54] Stefan Haeberle and Roland Zengerle. Microfluidic platforms for lab-on-a-chip applications. *Lab on a Chip*, 7(9):1094–1110, 2007.

[55] Akihiro Hattori and Kenji Yasuda. Evaluation of a centrifuged double y-shape microfluidic platform for simple continuous cell environment exchange. *International journal of molecular sciences*, 13(1):819–827, 2012.

[56] J Lundahl, G Hallden, M Hallgren, CM Sköld, and J Hed. Altered expression of cd11b/cd18 and cd62l on human monocytes after cell preparation procedures. *Journal of immunological methods*, 180(1):93–100, 1995.

[57] Hyunwoo Bang, Sun Hee Lim, Young Kyung Lee, Seok Chung, Chanil Chung, Dong-Chul Han, and Jun Keun Chang. Serial dilution microchip for cytotoxicity test. *Journal of Micromechanics and Microengineering*, 14(8):1165, 2004.

[58] Stephan KW Dertinger, Daniel T Chiu, Noo Li Jeon, and George M Whitesides. Generation of gradients having complex shapes using microfluidic networks. *Analytical Chemistry*, 73(6):1240–1246, 2001.

[59] David R Lide. *CRC handbook of chemistry and physics*. CRC press, 2004.

[60] DR Lide. Dr 2007-2008 crc handbook of chemistry and physics.

[61] Matthew A Holden, Saurabh Kumar, Edward T Castellana, Ali Beskok, and Paul S Cremer. Generating fixed concentration arrays in a microfluidic device. *Sensors and Actuators B: Chemical*, 92(1):199–207, 2003.

[62] Adrian T O'Neill, Nancy Monteiro-Riviere, and Glenn M Walker. A serial dilution microfluidic device for cytotoxicity assays. In *Engineering in Medicine and Biology Society, 2006. EMBS'06. 28th Annual International Conference of the IEEE*, pages 2836–2839. IEEE, 2006.

[63] Glenn M Walker, Nancy Monteiro-Riviere, Jillian Rouse, and Adrian T O'Neill. A linear dilution microfluidic device for cytotoxicity assays. *Lab on a Chip*, 7(2):226–232, 2007.

[64] Masumi Yamada, Takaya Hirano, Masahiro Yasuda, and Minoru Seki. A microfluidic flow distributor generating stepwise concentrations for high-throughput biochemical processing. *Lab on a Chip*, 6(2):179–184, 2006.

Appendix A

Appendices

A.1 Python code for controling the servo using Arduino microcontroller (Chapter 5)

```
#include <Servo.h>


Servo myservo;
int n = 0;
int nAngles = 13;
int delta = round((2330-550)/(nAngles-1));


void setup()
{
  Serial.begin(9600);
```

```
  pinMode(8, INPUT);
  pinMode(7, OUTPUT);
  myservo.attach(9);
  digitalWrite(7, HIGH);
}

void loop() {
  if(digitalRead(8) == HIGH) {
     Serial.println("detected HIGH");
     Serial.println(n);
     delay(1000);
     myservo.writeMicroseconds(2330-n*delta);  // set servo to 0 */

     Serial.println(2330-n*delta);
     n++;
     if(n>=nAngles) {
       n = 0;
     }
  }
}
```

A.2 Python code for Cell Trajectory (Chapter 8, Figure 26)

```
import numpy
import pylab, matplotlib
from matplotlib.patches import Rectangle


# Actual chip dimensions:  1 mm wide channel, 27 mm long channel.
# Actual bead radii:  3 um and 20 um


y_max = 1e-3          # channel height, m
R = y_max/2.0         # channel radius (half of the height), m
mu = 0.001            # viscosity, cP = kg m^-1 s^-1
g = -9.8
u_max = 100e-6        # maximum fluid velocity, m/s
delta_t = 1           # time interval between data points, s


###### tiny math for text in Introduction of paper:
###### this uses the smaller of the two particle sizes
that we simulate,
###### r=10 um, D=20 um
r_p = 10e-6 # 5 um particle radius, 20 um particle diameter
rho_p = 1010
rho_f = 1000
```

```
print "velocity in y direction ", (2.0/9.0) *
    (g * r_p**2 * (rho_p-rho_f))/mu



def plot_setup(facecolors):
    matplotlib.rcParams.update({'font.size': 30})
    pylab.figure(num=None, figsize=(25, 4), dpi=80,
        facecolor='w', edgecolor='k')
    pylab.subplots_adjust(left=0.10, right=0.99,
        top=0.97, bottom=0.25)
    currentAxis = pylab.gca()
    currentAxis.add_patch(Rectangle((-3, 0),
        30, 1e6*y_max*1/3, alpha=1, facecolor=facecolors[0]))
    currentAxis.add_patch(Rectangle((-3, 1e6*y_max*1/3),
        30, 1e6*y_max*1/3, alpha=1, facecolor=facecolors[1]))
    currentAxis.add_patch(Rectangle((-3, 1e6*y_max*2/3),
        30, 1e6*y_max*1/3, alpha=1, facecolor=facecolors[2]))
    pylab.xlabel("Location along channel length (mm)")
    pylab.ylabel("Location along\nchannel height\n($\mu$m)")
    # super awesome parabolic flow arrows creator:
    ys=range(0,1100,100)
    for y in ys:
```

```
        r = (y - R*1e6)  # used to have abs()
        u_x = 1.5 * (1 - (r/(R*1e6))**2)
        pylab.arrow(-2,y,u_x,0, head_width=50,
            head_length=0.1, fc='k', ec='k')


def sim(r_p, rho_p, rho_f1, rho_f2, rho_f3, c, ms):
    neutrally_buoyant = False
    t=0
    x=[]
    y=[]
    for i in range(10000):
        if i == 0:
            # for the first point, just put the particle at....
             the starting point (0,y_max):
            x.append(0)
            y.append(y_max)
        else:
            # calculate new x location: (used to have abs())
            r = (y[i-1] - R)
            u_x = u_max * (1 - (r/R)**2)
            x.append(x[i-1] + u_x * delta_t)
```

```
        # calculate new y location:
        if neutrally_buoyant:
            y.append(y[i-1])
        else:
            if y[i-1] > y_max * 2.0 / 3.0:
                rho_f = rho_f1
            elif y[i-1] > y_max * 1.0 / 3.0:
                rho_f = rho_f2
            else:
                rho_f = rho_f3
            u_y = (2.0/9.0) * (g * r_p**2 * (rho_p-rho_f))/mu
            y.append(y[i-1] + u_y * delta_t)
            if y[i] > y[i-1]:
                # test for neutral buoyancy
                # Warning, this only works with
                # particles that are initially sinkers
                neutrally_buoyant = True
                # replace latest point with copy of
                # previous point to avoid bounce
                y[i] = y[i-1]
    t += delta_t
    # if the particle has hit the bottom of the channel, stop:
```

```
            if y[i] < 0:
                break
            # this sets how far out in time you're simulating
            if i > 1000:
                break
        pylab.plot(numpy.array(x)*1e3,numpy.array(y)*1e6, 'o',
            ms=ms, c=c, markevery=5, alpha=1, markeredgewidth=2)


plot_setup(['#6666ff', '#9999ff', '#ccccff'])
sim(r_p=20e-6, rho_p=1060.0, rho_f1=1050.0, rho_f2=1070.0,
    rho_f3=1090.0, c="g", ms=20)
sim(r_p=10e-6, rho_p=1060.0, rho_f1=1050.0, rho_f2=1070.0,
    rho_f3=1090.0, c="g", ms=10)
sim(r_p=20e-6, rho_p=1080.0, rho_f1=1050.0, rho_f2=1070.0,
    rho_f3=1090.0, c="r", ms=20)
sim(r_p=10e-6, rho_p=1080.0, rho_f1=1050.0, rho_f2=1070.0,
    rho_f3=1090.0, c="r", ms=10)
pylab.xlim([-2.5,25])
pylab.ylim([-70,y_max*1e6+70])  # plot just the channel region
pylab.yticks([0,500,1000])
pylab.savefig("out1.pdf")
pylab.cla()
```

```
plot_setup(['#ccccff', '#ccccff', '#ccccff'])
sim(r_p=20e-6, rho_p=1060.0, rho_f1=1050.0, rho_f2=1050.0,
    rho_f3=1050.0, c="g", ms=20)
sim(r_p=10e-6, rho_p=1060.0, rho_f1=1050.0, rho_f2=1050.0,
    rho_f3=1050.0, c="g", ms=10)
sim(r_p=20e-6, rho_p=1080.0, rho_f1=1050.0, rho_f2=1050.0,
    rho_f3=1050.0, c="r", ms=20)
sim(r_p=10e-6, rho_p=1080.0, rho_f1=1050.0, rho_f2=1050.0,
    rho_f3=1050.0, c="r", ms=10)
pylab.xlim([-2.5,25])
pylab.ylim([-70,y_max*1e6+70])  # plot just the channel region
pylab.yticks([0,500,1000])
pylab.savefig("out2.pdf")
```

A.3 MATLAB code for Cell Trajectory (Chapter 8, Figure 26)

```
%% calculation of particle's distance for single layer density
clear
figure
```

```
plot([0 100],[0.335 0.335],'Color', ...
    [135 206 250]/256, 'linewidth', 190)
hold on
plot([0 100],[0 0],'Color', [0 191 255]/256, 'linewidth', 113)
plot([0 100],[-0.335 -0.335],'color', ...
    [30 144 255]/256, 'linewidth', 115.5)
hold on
grid on


% Yellow particle (1.06 kg/m^3, r=20um)
g=9.8; % m/s^2
mu= 0.001; %kg/m*s
rhoc=1060;  %kg/m^3
rhof=1050;  %kg/m^3
rhof1=1070;  %kg/m^3
rhof2=1090;
r=0.000020; % meter
h=0.0005; %mm
Q=4; %mm^3/min
D=1; %mm
A= (pi*D^2)/4; % mm^2
```

```
Vy=((2/9)*((rhoc-rhof)/mu)*g*(r^2));
Vm= ((Q/A)/(60)/(1000));

%Vy=Vy*(-1)
if (Vy>0)

    D = D/1000; % convert D from mm to m
    T= D/Vy;
    delta=T/50;

    R = D/2;

    colr=['g', 'b', 'b', 'c'];
    m = 1;
    he =40;

    y(1)=he*D/100;
    x(1)=0;
    n=1;
    while (y(n) > -5e-4)
        y(n+1)=y(n)-Vy*delta;
        x(n+1)=x(n)+Vm*(1-(y(n+1)/R)^2)*delta;
```

```
    if ((y(n+1) < 1.7e-4) & (y(n+1) > -1.6e-4))
        Vy=((2/9)*((rhoc-rhof1)/mu)*g*(r^2));
        if (rhoc < rhof1)
            break;
        end
    elseif(y(n+1) < -1.6e-4)
        Vy=((2/9)*((rhoc-rhof2)/mu)*g*(r^2));
        if (rhoc < rhof2)
            break;
        end
    end
    n = n+1;

end
plot(x*1000,y*1000, 'yo','MarkerSize',15,...
    'MarkerEdgeColor','k','MarkerFaceColor','y')

hold on
plot (x(end)*1000:0.37:100,y(end)*1000,...
    'yo','MarkerSize',15,'MarkerEdgeColor',...
    'k','MarkerFaceColor','y')
```

```
end

m = m +1;

hold on

% Yellow particle (1.06 kg/m^3, r=3um)
g=9.8; % m/s^2
mu= 0.001; %kg/m*s
rhoc=1060;  %kg/m^3
rhof=1050;  %kg/m^3
rhof1=1070;  %kg/m^3
rhof2=1090;
r=0.000003; % meter
h=0.0005; %mm
Q=1; %mm^3/min
D=1; %mm
A= (pi*D^2)/4; % mm^2

Vy=((2/9)*((rhoc-rhof)/mu)*g*(r^2));
Vm= ((Q/A)/(60)/(1000));
```

```
if (Vy>0)

    D = D/1000; % convert D from mm to m
    T= D/Vy;
    delta=T/175;

    R = D/2;
    colr=['b', 'g', 'm', 'c'];
    m = 1;
    he =40;

    y(1)=he*D/100;
    x(1)=0;
    n=1;
    while (y(n) > -5e-4)
        y(n+1)=y(n)-Vy*delta;
        x(n+1)=x(n)+Vm*(1-(y(n+1)/R)^2)*delta;

        if ((y(n+1) < 1.7e-4) & (y(n+1) > -1.6e-4))
            Vy=((2/9)*((rhoc-rhof1)/mu)*g*(r^2));
            if (rhoc < rhof1)
```

```
                break;
            end
        elseif(y(n+1) < -1.6e-4)
            Vy=((2/9)*((rhoc-rhof2)/mu)*g*(r^2));
            if (rhoc < rhof2)
                break;
            end
        end
        n = n+1;

    end
    plot(x*1000,y*1000, 'yo','MarkerSize',5,...
        'MarkerFaceColor','y','MarkerEdgeColor','k')

    hold on
    plot (x(end)*1000:0.23:100,y(end)*1000,...
        'yo','MarkerSize',5,'MarkerEdgeColor','...
        k','MarkerFaceColor','y')

end
m = m +1;
```

```
hold on;

clear y;

clear x;



% Red particle (1.06 kg/m^3, r=20um)

g=9.8; % m/s^2

mu= 0.001; %kg/m*s

rhoc=1080;  %kg/m^3

rhof=1050;  %kg/m^3

rhof1=1070;  %kg/m^3

rhof2=1090;

r=0.000020; % meter

h=0.0005; %mm

Q=1; %mm^3/min

D=1; %mm

A= (pi*D^2)/4; % mm^2


Vy=((2/9)*((rhoc-rhof)/mu)*g*(r^2));

Vm= ((Q/A)/(60)/(1000));


if (Vy>0)
```

```
D = D/1000; % convert D from mm to m

T= D/Vy;

delta=T/34;


R = D/2;


colr=['c', 'g', 'm', 'r'];

m = 1;

he =40;


y(1)=he*D/100;

x(1)=0;

n=1;

while (y(n) > -5e-4)

    y(n+1)=y(n)-Vy*delta;

    x(n+1)=x(n)+Vm*(1-(y(n+1)/R)^2)*delta;


    if ((y(n+1) < 1.7e-4) & (y(n+1) > -1.6e-4))

        Vy=((2/9)*((rhoc-rhof1)/mu)*g*(r^2));

        delta=T/10;
```

```
            if (rhoc < rhof1)
                break;
            end
        elseif(y(n+1) < -1.6e-4)
            Vy=((2/9)*((rhoc-rhof2)/mu)*g*(r^2));

            if (rhoc < rhof2)
                break;
            end
        end
        n = n+1;

    end
    plot(x*1000,y*1000, 'ro','MarkerSize',...
        15,'MarkerEdgeColor','r','MarkerFaceColor',...
        'r','MarkerEdgeColor','k')
    plot (x(end)*1000:0.4:100,y(end)*1000,...
        'ro','MarkerSize',15,'MarkerEdgeColor','k',....
        'MarkerFaceColor','r')

end
```

```
m  = m +1;
hold on


g=9.8; % m/s^2
mu= 0.001; %kg/m*s
rhoc=1080;  %kg/m^3
rhof=1050;  %kg/m^3
rhof1=1070;  %kg/m^3
rhof2=1090;
r=0.000003; % meter
h=0.0005; %mm
Q=1; %mm^3/min
D=1; %mm
A= (pi*D^2)/4; % mm^2


Vy=((2/9)*((rhoc-rhof)/mu)*g*(r^2));
Vm= ((Q/A)/(60)/(1000));
if (Vy>0)


    D = D/1000; % convert D from mm to m
    T= D/Vy;
    delta=T/87;
```

```
R = D/2;
colr=['m', 'g', 'k', 'b'];
m = 1;
he =40;

y(1)=he*D/100;
x(1)=0;
n=1;
while (y(n) > -5e-4)
    y(n+1)=y(n)-Vy*delta;
    x(n+1)=x(n)+Vm*(1-(y(n+1)/R)^2)*delta;

    if ((y(n+1) < 1.7e-4) & (y(n+1) > -1.6e-4))
        Vy=((2/9)*((rhoc-rhof1)/mu)*g*(r^2));
        if (rhoc < rhof1)
            break;
        end
    elseif(y(n+1) < -1.6e-4)
        Vy=((2/9)*((rhoc-rhof2)/mu)*g*(r^2));
        if (rhoc < rhof2)
            break;
```

```
            end
        end
        n = n+1;

    end
    plot(x*1000,y*1000,'ro','MarkerSize',5,...
        'MarkerEdgeColor','k','MarkerFaceColor','r'
    hold on
    plot (x(end)*1000:0.23:100,y(end)*1000,...
        'ro','MarkerSize',5,'MarkerEdgeColor','k',...
        'MarkerFaceColor','r')
end
m = m +1;
hold on
ylim([-0.5 0.5])
xlim([0 50]);
grid on
grid on
    xlabel('Microsphere trajectory in x-direction (mm)...
        ','fontweight', 'bold','FontSize',14.5);
    ylabel('Microsphere trajectory in y-direction (mm)...
        ','fontweight', 'bold','FontSize', 14);
```

```
    title ('Microsphere trajectory in 3 density layers...
          (1.050, 1.070, 1.090 g/mL)',...
          'fontweight','bold','FontSize',16);


% calculation of particle's distance for single layer density

clear
figure

plot([0 100],[0 0],'Color', [135 206 250]/256, 'linewidth', 715)
hold on
grid on

g=9.8; % m/s^2
mu= 0.001; %kg/m*s
rhoc=1060;  %kg/m^3
rhof=1050;  %kg/m^3
%rhof1=1070;  %kg/m^3
%rhof2=1090;
r=0.000003; % meter
%h=0.0004; %mm
```

```
Q=0.4; %mm^3/min
D=1; %mm
A= (pi*D^2)/4; % mm^2

    Vy=((2/9)*((rhoc-rhof)/mu)*g*(r^2));
    Vm= ((Q/A)/(60)/(1000));
%
if (Vy>0)

    D = D/1000; % convert D from mm to m
    T= D/Vy;
    delta=T/35;

    R = D/2;
    he=40;
    y(1)=he*D/100;
    x(1)=0;

    n=1;
    for t=0:delta:T;
        y(n+1)=y(n)-Vy*delta;
        x(n+1)=x(n)+Vm*(1-(y(n+1)/R)^2)*delta;
```

```
        n = n+1;
    end

    plot(x*1000,y*1000, 'bo','MarkerSize',5,...
        'MarkerEdgeColor','b',...
    'MarkerFaceColor',[.49 1 .63])
    plot(x*1000,y*1000, 'yo','MarkerSize',5,...
        'MarkerFaceColor','y','MarkerEdgeColor','k')

end

hold on

X = x(end);
Y = y(end);



g=9.8; % m/s^2
mu= 0.001; %kg/m*s
rhoc=1060;  %kg/m^3
rhof=1050;  %kg/m^3
%rhof1=1070;  %kg/m^3
```

```
%rhof2=1090;
r=0.000020; % meter
h=0.0004; %mm
Q=1; %mm^3/min
D=1; %mm
A= (pi*D^2)/4; % mm^2

    Vy=((2/9)*((rhoc-rhof)/mu)*g*(r^2));
    Vm= ((Q/A)/(60)/(1000));
%
if (Vy>0)

    D = D/1000; % convert D from mm to m
    T= D/Vy;
    delta=T/50;

    R = D/2;
     he=40;
    y(1)=he*D/100;
    x(1)=0;
    n=1;
    for t=0:delta:T;
```

```
        y(n+1)=y(n)-Vy*delta;
        x(n+1)=x(n)+Vm*(1-(y(n+1)/R)^2)*delta;
        n = n+1;
    end
    plot(x*1000,y*1000, 'yo','MarkerSize',15,...
        'MarkerEdgeColor','k','MarkerFaceColor','y')
    hold on
    plot(x*1000,y*1000, 'yo','MarkerSize',15,...
        'MarkerFaceColor','y','MarkerEdgeColor','k')
end
hold on
X = x(end);
Y = y(end);
clear;


g=9.8; % m/s^2
mu= 0.001; %kg/m*s
rhoc=1080;  %kg/m^3
rhof=1050;  %kg/m^3
%rhof1=1070;  %kg/m^3
%rhof2=1090;
r=0.000003; % meter
```

```
h=0.0004; %mm
Q=1; %mm^3/min
D=1; %mm
A= (pi*D^2)/4; % mm^2

    Vy=((2/9)*((rhoc-rhof)/mu)*g*(r^2));
    Vm= ((Q/A)/(60)/(1000));
%
if (Vy>0)
     D = D/1000; % convert D from mm to m
    T= D/Vy;
    delta=T/35;
    R = D/2;
     he=40;
    y(1)=he*D/100;
    x(1)=0;
    n=1;
    for t=0:delta:T;
        y(n+1)=y(n)-Vy*delta;
        x(n+1)=x(n)+Vm*(1-(y(n+1)/R)^2)*delta;
        n = n+1;
    end
```

```
    plot(x*1000,y*1000, 'ro','MarkerSize',5,...
        'MarkerEdgeColor','k','MarkerFaceColor','r')
    hold on
    plot(x*1000,y*1000, 'ro','MarkerSize',5,...
        'MarkerFaceColor','r','MarkerEdgeColor','k')
  end

hold on

X = x(end);
Y = y(end);

g=9.8; % m/s^2
mu= 0.001; %kg/m*s
rhoc=1080;  %kg/m^3
rhof=1050;  %kg/m^3
%rhof1=1070;  %kg/m^3
%rhof2=1090;
r=0.000020; % meter
h=0.0004; %mm
Q=1; %mm^3/min
D=1; %mm
```

```
A= (pi*D^2)/4; % mm^2
    Vy=((2/9)*((rhoc-rhof)/mu)*g*(r^2));
    Vm= ((Q/A)/(60)/(1000));
if (Vy>0)
    D = D/1000; % convert D from mm to m
    T= D/Vy;
    delta=T/50;

    R = D/2;
     he=40;
    y(1)=he*D/100;
    x(1)=0;
    n=1;
    for t=0:delta:T;
        y(n+1)=y(n)-Vy*delta;
        x(n+1)=x(n)+Vm*(1-(y(n+1)/R)^2)*delta;
        n = n+1;
    end
      plot(x*1000,y*1000, 'ro','MarkerSize',15,...
          'MarkerEdgeColor','k','MarkerFaceColor','r')
   hold on
   plot(x*1000,y*1000, 'ro','MarkerSize',15,...
```

```
        'MarkerFaceColor','r','MarkerEdgeColor','k')
end
ylim([-0.5 0.5])
xlim([0 50]);
grid on
xlabel('Microsphere trajectory in x-direction (mm)',...
    'fontweight', 'bold','FontSize',14);
ylabel('Microsphere trajectory in y-direction (mm)',...
        'fontweight', 'bold','FontSize', 14);
title ('Microsphere trajectory in 1 density layer...
        (1.050 g/mL)','fontweight', ...
    'bold','FontSize',16);
```